**Mutations in *CLPB* cause intellectual disability, congenital neutropenia, progressive brain atrophy, movement disorder, cataracts and 3-methylglutaconic aciduria**

Running title: CLPB defect

Saskia B. Wortmann[1], Szymon Ziętkiewicz[2]*, Maria Kousi[3]*, Radek Szklarczyk[4]*, Tobias B. Haack[5,6], Sören Gersting[7], Ania Muntau[7], Aleksandar Rakovic[8], G. Herma Renkema[1], Richard Rodenburg[1], Tim M. Storm[5], Thomas Meitinger[5], M Estela Rubio-Gozalbo[9], Elzbieta Chrusciel[2], Felix Distelmaier[10], Christelle Golzio[3], Joop H. Jansen[11], Clara van Karnebeek[12,13], Yolanda Lillquist[12,13], Thomas Lücke[14], Katrin Õunap[15], Riina Zordania[15], Joy Yaplito-Lee[16], Hans van Bokhoven[17], Johannes N. Spelbrink[1,18], Frédéric M. Vaz[19], Mia Pras-Raves[19], Rafal Ploski[20] Ewa Pronicka[21], Christine Klein[8], Michel A.A.P. Willemsen[22], Arjan P.M. de Brouwer[17,23], Holger Prokisch[5], Nicholas Katsanis[3], Ron A. Wevers[24]

*equal contributions

[1] Nijmegen Centre for Mitochondrial Disorders (NCMD), Amalia Children's Hospital, RadboudUMC Nijmegen, The Netherlands

[2] Department of Molecular and Cellular Biology, Intercollegiate Faculty of Biotechnology, University of Gdańsk, Poland

[3] Center for Human Disease Modeling, Duke University Medical Center, Durham, NC, USA

[4] Clinical Genomics, Maastricht UMC+, Maastricht, The Netherlands

[5] Institute of Human Genetics, Helmholtz Zentrum Munich, Neuherberg, Germany

[6] Institute of Human Genetics, Technische Universität München, Munich, Germany

[7] Department of Molecular Pediatrics, Dr. von Hauner Children's Hospital, Ludwig-Maximilians-University, Munich, Germany.

[8] Institute of Neurogenetics, University of Lübeck, Lübeck, Germany

[9] Departments of Pediatrics and Genetic Metabolic Diseases, Maastricht University Medical Center, Maastricht, The Netherlands

[10] Department of General Pediatrics, Neonatology and Pediatric Cardiology, University Children's Hospital, Heinrich-Heine University, Düsseldorf, Germany

[11] Department of Laboratory Medicine, Laboratory of Hematology, RadboudUMC, Nijmegen, The Netherlands

[12] Division of Biochemical Diseases, Department of Pediatrics, B.C. Children's Hospital, Canada; Treatable Intellectual Disability Endeavour, British Columbia, Canada

[13] Child and Family Research Institute, Centre for Molecular Medicine & Therapeutics, Canada; University of British Columbia, Vancouver, Canada
[14] Department of Neuropediatrics, University Children's Hospital, Ruhr University, Bochum, Germany.
[15] Department of Genetics, United Laboratories, Tartu University Hospital, Tartu, Estonia
[16]Metabolic Genetics, Murdoch Childrens Research Institute, Royal Children's Hospital, Parkville, VIC 3052, Australia.
[17]Department of Human Genetics, RadboudUMC Nijmegen, The Netherlands
[18] BioMediTech, FI-33014 University of Tampere, Tampere, Finland
[19] Department of Clinical Chemistry and Pediatrics, Laboratory Genetic Metabolic Disease, Academic Medical Center, Amsterdam, The Netherlands
[20] Department of Medical Genetics, Warsaw Medical University, Warsaw, Poland
[21] Department of Metabolic Diseases, Children's Memorial Health Institute Warsaw, Poland
[22] Department of Neurology, RadboudUMC Nijmegen, The Netherlands
[23]Department of Cognitive Neurosciences, Donders Institute for Brain, Cognition and Behaviour, Radboud University Nijmegen, Nijmegen, The Netherlands
[24] Department of Laboratory Medicine, Translational Metabolic Laboratory, RadboudUMC, Nijmegen, The Netherlands

[+]Correspondence:
S.B. Wortmann, Amalia Children's Hospital, RadboudUMC, internal postal code 804, P.O Box 9101, 6500 HB Nijmegen, The Netherlands. fax+31-(0)24-3616428, voice +31-(0)24-3614430.
saskia.wortmann-hagemann@radboudumc.nl

**Author contributions**

SW, RW designed and supervised the study.

SW characterized the syndrome, collected clinical data and individual tissues.

MERG, FD, CvK, YL, TL, KO RZ, JYL, EP referred individuals.

SW, RS, TH, RR, RP, HP, HvB, TS, TM performed the genetic studies and identified the causative genetic defect.

FV, MPR performed the phospholipid spectra analysis and interpreted the data.

CK, AR performed and interpreted the studies on auto-/mitophagy.

GHR, JS performed immune fluorescence and western blotting studies on ClpB.

RR performed and interpreted the oxidative phosphorylation measurements.

MK, CG, NK designed, performed and interpreted the *in vivo* functional experiments.

SZ, EC designed, performed and interpreted *in vitro* biochemical experiments and purified proteins.

RS, SZ, AdB interpreted the effects of the mutations on protein level, analysed the protein structure and predicted the function in human.

SW, JJ interpreted the haematological data.

SW, MW interpreted the neurological data.

SG, AM evaluated the protein protein interactions.

All authors contributed to the draft manuscript.

SW, AdB, NK, RW prepared the final manuscript**.**

**Competing financial interests**

The authors declare no competing financial interests.

**Abstract**

We studied a group of individuals with elevated urinary excretion of 3-methylglutaconic acid, neutropenia that can develop into leukemia, a neurological phenotype ranging from non-progressive intellectual disability to a prenatal encephalopathy with progressive brain atrophy, movement disorder, cataracts, and early death. Exome sequencing of two unrelated individuals identified a total of 14 rare, predicted deleterious alleles in *CLPB* in 14 individuals from nine unrelated families. *CLPB* encodes caseinolytic peptidase B homolog ClpB, a member of the AAA+ protein family. To evaluate the relevance of CLPB in the pathogenesis of this syndrome, we developed a zebrafish model and an *in vitro* assay to measure ATPase activity. Suppression of *clpb* in zebrafish embryos induced a central nervous system phenotype that was consistent with cerebellar and cerebral atrophy that could be rescued by wild-type, but not mutant human *CLPB* mRNA. Consistent with these data, the loss-of-function effect of one of the identified variants (p.Arg408Gly) was supported further by *in vitro* evidence with the mutant peptides abolishing ATPase function. Additionally, we show that CLPB interacts biochemically with ATP2A2, known to be involved in apoptotic processes in severe congenital neutropenia (SCN) 3 (Kostmann disease (*HAX1*)). Taken together, mutations in *CLPB* define a syndrome with intellectual disability, congenital neutropenia, progressive brain atrophy, movement disorder, cataracts and 3-methylglutaconic aciduria.

**Keywords**

AAA+ protein superfamily, *AGK*, Barth syndrome, inborn error of metabolism, MEGDEL syndrome, *SERAC1, TAZ*, 3-MGA

## Introduction

The implementation of exome (ES) and genome sequencing has expanded our knowledge of genes that cause pediatric syndromic phenotypes. Nonetheless, of the affected individuals sequenced under a suspected genetic etiology hypothesis, 50-75% do not yield a definitive molecular diagnosis, highlighting the number of causal genes still at large [1; 2]. For a subset of these individuals, clinical management can be assisted by findings from metabolic markers in blood and urine that might point towards hitherto unappreciated inborn errors of metabolism (IEM).

The 3-methylglutaconic acid (3-MGA) detected in urine samples is such a marker, showing consistently and significantly elevated levels in a rapidly growing group of IEM with a syndromic phenotype [3]. This group encompasses several disorders in which phospholipid remodeling and other mitochondrial membrane-related processes are defective. Clinical features are heterogeneous but distinctive. For example, Barth syndrome, caused by mutations in *TAZ* (MIM #306030), is associated with (cardio)myopathy, neutropenia, and delayed motor milestones; Sengers syndrome, driven by mutations in *AGK* (MIM#212350), manifests cardiomyopathy and cataracts; and MEGDEL syndrome, caused by mutations in *SERAC1* (MIM#614739), is associated with deafness and dystonia[4]. In addition, congenital neutropenia and central nervous system involvement have also been reported in disorders without 3-MGA, such as Kostmann syndrome (*HAX1,* MIM #610738), Shwachman-Bodian-Diamond disease (*SDBS*, MIM #260400), and Cohen syndrome (*VPS13B,* MIM#216550) [5].

Here we present a constellation of pathologies that cannot be reconciled with any known clinical entity. This phenotypic spectrum encompasses intellectual disability (ID)/ developmental delay (DD); congenital neutropenia; progressive brain atrophy; movement disorder; and bilateral cataracts. Though all individuals share 3-MGA-uria as a characteristic biomarker, the severity of the other signs and symptoms shows inter-individual variability. Nonetheless, under the hypothesis that the consistently observed metabolic signature underpins a discrete molecular genetic disorder, we performed ES in two unrelated individuals, followed by subsequent candidate gene testing in a further 16 affected individuals. Through these studies, the implementation of an *in vivo* model that recapitulated key neuroanatomical aspects of the disorder, and biochemical *in vitro* testing, we report the identification of loss of function mutations in *CLPB*.

## Methods

### Clinical cohort

Individuals 6 and 9 manifested an overlapping phenotype of ID, neutropenia, cataracts and 3-MGA-uria and were independently evaluated by ES at two different centers (RadboudUMC, Nijmegen, The Netherlands; Helmholtz Zentrum Munich, Germany). After identification of the genetic defect in these cases, we selected 16 additional individuals with an overlapping clinical presentation from the internal database at RadboudUMC. This study adhered to the Declaration of Helsinki and written informed consent was obtained from each individual.

### Exome sequencing and variant identification

ES for individual 6 was performed as previously described [6]. In brief, we used a SureSelect Human All Exon 50 Mb Kit (Agilent) for enrichment and a HiSeq2500 (Illumina). Reads were aligned to the human reference assembly (hg19) with BWA (version 0.5.8). More than 90% of the exome was covered at least 20×. Single-nucleotide variants (SNVs) and small insertions and deletions were detected with SAMtools (version 0.1.7). Variant prioritization was performed based on an autosomal-recessive pattern of inheritance. ES for individual 9 was performed as previously described with minor adjustments [7]. In brief, we used the SureSelectXT Human All Exon 50Mb Kit (Agilent) for enrichment and a SOLiD 5500XL (Life TechnologiesTM). We excluded all non-genic, intronic (other than canonical splice sites) and synonymous variants, and all known variants with a frequency > 1% in dbSNPv132 and our in-house variant database consisting of 672 exomes. Next, as a recessive disease model was expected and given the assumption of a common ancestral allele (based on parental consanguinity), we prioritized variants according the percentage of variant reads. For this, we used the threshold of >75% variant reads as an indicator for homozygous variants.

### Mutation analysis by Sanger sequencing

Primer sequences for amplification of all protein coding exons of *CLPB* (GenBank ID NM_030813.4) are shown in **Table S1**. PCR conditions are available upon request. PCR products were sequenced using the ABI PRISM BigDye Terminator Cycle Sequencing V2.0 Ready Reaction Kit and analyzed with the ABI PRISM 3730 DNA analyzer (Applied Biosystems, Foster City, USA).

### *In vivo* functional modeling of *CLPB* mutations in zebrafish

Zebrafish embryos and adults were maintained and mated as described and all experiments were carried out with the approval of the Institutional Animal Care and Use Committee (IACUC)[8]. For the *in vivo* complementation experiments a translational-blocking morpholino (MO) against the sole zebrafish *clpb* ortholog was designed (**Figure S1**) and obtained from Gene Tools, LLC. We injected 1nl of diluted MO (2.5 ng) and/or RNA (200 pg for WT or mutant *clpb*) into wildtype zebrafish embryos at the 1-to 4-cell stage. For acetylated tubulin staining marking the neuronal axon processes, injected embryos were treated as described[9]. For RNA rescue and overexpression experiments, the human wild type mRNA of the canonical isoform (NM_030813.4) of *CLPB* was cloned into the pCS2+ vector and transcribed *in vitro* using the SP6 Message Machine kit (Ambion). The four variants tested, p.R408G, p.M411I, p.Y617C and p.G646V, were introduced using Phusion high-fidelity DNA polymerase (New England Biolabs) and custom-designed primers. Image acquisition and analysis was performed using Nikon NIS-Elements Advanced Research software. All experiments were repeated in triplicate and significance of the morphant phenotype was judged using student`s $\chi^2$-test.

**Purification and biochemical characterization of human CLPB**

The CLPBΔN92 construct (deletion of predicted signal peptide) was PCR-generated using a pENTR223-hCLPB plasmid as a template. The amplified DNA fragment was cloned into the pET15b vector (Novagen) at the *Nde* I/*Bam* HI sites, resulting in a construct pET15b-CLPBΔN92 with an introduced N-terminal His-tag. The construct was verified by DNA sequencing. The p.Arg408Gly mutation of CLPBΔN92 was introduced into pET15b-CLPBΔN92 by site-directed mutagenesis, and confirmed by DNA sequencing.

The CLPBΔN92 and its p.Arg408Gly variant were expressed in *E. coli* BL21(DE3). Pelleted cells were diluted 1/1 (v/v) with buffer (NaCl 300 mM, imidazole 20 mM, glycerol 20%, 2-mercaptoethanol 5 mM, HEPES 20 mM, pH 7.4), French press lysed and centrifuged at 75000g for 1 h. The lysate was incubated with 2 ml Ni-NTA resin in batch mode. After washing with buffer (NaCl 150 mM, imidazole 20 mM, glycerol 20%, 2-mercaptoethanol 5 mM, HEPES 40 mM, pH 7.4) and then with the same buffer supplemented with 48 mM imidazole, proteins were eluted with 300 mM pure imidazole and applied on a PD10 desalting column equilibrated with buffer without imidazole (the other components of washing-, elution- and desalting buffers remained the same). Protein identity was confirmed by Western blot, using an anti-CLPB antibody (Abcam, ab87253) **(Figure S2A). Figure S2B** shows purified CLPB_WT and the purified CLPB_p.Arg408Gly on SDS-PAGE. Protein

concentrations were estimated by Coomassie-stained SDS-PAGE gel densitometry using BSA as a standard. The ATPase activity of purified human CLPB (CLPB_WT) and its p.Arg408Gly mutant (CLPB_p.Arg408Gly) was analyzed using the coupled pyruvate kinase/lactate dehydrogenase assay, as previously described [10]. 2 µM hCLPB were incubated with 20 mM ATP at 36 $^{o}$C and the absorbance change was recorded at 1 sec intervals. The rate was calculated from the linear part of the curve (steady state rate). For WT hCLPB the measurement was additionally performed in the presence of casein (0.2 mg/ml).

## Results

### The phenotypic spectrum of individuals with mutations in *CLPB*

The clinical presentation and course of the 14 affected individuals (eight females, six males) varied substantially from a mild phenotype (individuals #1,2) associated with cataracts and neutropenia but no neurological involvement or infections, to the most severe phenotype (individuals #9-14) associated with neonatal or even prenatal onset of neurological symptoms (progressive brain atrophy, absence of development, movement disorder, seizures), severe neutropenia with progression into leukemia and death in the first months of life. The detailed clinical histories of the cohort can be found in the **Supplementary data** and are summarized in **Table 1, Figures 1 and 2**. Common features include ID/DD (12/14 individuals investigated), congenital neutropenia (10/14), brain atrophy (7/9), microcephaly (7/12), movement disorder (7/13); cataracts (5/10) and 3-MGA-uria (12/12 individuals). The oldest affected participant alive is 18 years old, the youngest 2 years old. Six individuals passed away between the ages of 24 days and 46 months.

*Neurological phenotype*

Two individuals (# 1, 2), currently aged eight and ten years, showed no neurological involvement at all as determined by a normal neurological examination, normal IQ test, and, in one person, normal brain imaging. However, individual #1 had ADHD, dyslexia, and dysgraphia; individual #2 had a tendency to impulsivity. All other persons (#3-14) showed DD/ID; the most severe cases (# 10-14) did not develop at all, did not make any eye or other contact, and suffered from (episodic to permanent) unconsciousness from birth until their early death. Most of them (individuals #3-14) showed pyramidal tract involvement, progressing from severe hypotonia during the first months of life to severe bilateral spasticity thereafter. In the most severe cases (individuals #12-14) these degenerative processes likely started during fetal life, since all individuals were born as “stiff babies” with generalized increased muscle tension including contractures and jaw lock. Additionally, 11 individuals suffered swallowing difficulties, potentially of both muscular and central nervous origin, necessitating tube feeding. In four individuals, epilepsy was reported. Furthermore, there is a spectrum of MRI abnormalities ranging from isolated cerebellar atrophy (#6, **Figure 1J**) in less severely affected individuals to atrophy of both cerebral hemispheres, the basal ganglia, and the cerebellum, in the most severely affected persons **(Figure 1E-H).** Additionally, white matter involvement was seen in individuals #7, 8, 9 and 11. The brain atrophy corresponds

with the clinical finding of microcephaly in seven of 12 investigated persons. In the individuals with basal ganglia involvement (#7, 8, 9) clinically-established dystonia was observed.

*Hematological/ immunological phenotype*

Neutropenia was noted in 10 of the 14 individuals being chronic severe (<0.5 G/L) in six (#1, 9, 10, 11, 13, 14) and moderate (0.5-1.0 G/L) in three (#2, 6, 12). One person (#3) was only found to be neutropenic subsequent to infections, the severity of which, appear concomitant with the severity of the neurological phenotype. Whereas individuals without neurological symptoms (#1, 2) did not suffer from recurrent infections, individuals #3-8 suffered from more frequent infections than peers but without serious complications. The remaining individuals from the study cohort (#9-14) suffered regularly from serious, often life-threatening infections and were treated with G-CSF (#9 and 12, during infections also #3), continuous antibiotics and antimycotics (see **Figure 2A** for details on neutropenia of #9). The bone marrow examination of individual #9 showed a maturation arrest at the stage of the promyelocyte **(Figure 2B, C).** In addition, we observed an absence of mature neutrophils in the bone marrow of individuals #10 and 11. Of note, two siblings, who were not treated with G-CSF, progressed to (i) an acute myeloid leukemia (M5, acute monocytic, with the typical finding of a somatic monosomy of chromosome 7; individual #10) or a (ii) myelodysplastic syndrome/preleukemia of myelomonocytic type (participant #11), respectively. Chemotherapeutic treatment was initiated in individual #10, who died shortly after. No treatment was initiated in individual #11, who also died shortly after the diagnosis. Bone marrow aspiration in the third available individual (# 13) showed a vacuolar degeneration of the phagocytic mononuclear system without typical signs of neutropenia.

*Other signs and symptoms*

For ten of the study participants, information about ophthalmological findings was available. Five of these individuals had bilateral cataracts, one (#7) was diagnosed with a suspected pigmentary retinopathy. Two individuals showed cardiac involvement, namely mild septal hypertrophy (#7) and mild dilated cardiomyopathy (#14). Two study participants had peripheral endocrine abnormalities (#6 and 7). At least three individuals (#9, 10, 11) showed similar facial dysmorphisms (e.g. low nasal bridge, hypertelorism, tented mouth, **Figure 1B, C**). From a biochemical standpoint, no consistently elevated serum lactate or alanine were observed in any of the investigated individuals, nor did they have an elevated urinary

excretion of Krebs cycle intermediates. All individuals had consistent and significant excretion of 3-MGA in their urine, amounting to 2-15 times over the limit of the reference range pointing to a possible mitochondrial dysfunction. It was observed that the concentration of this biomarker could fluctuate in an individual (#2: 29-109 (reference <12 µmol/mmol creatinine); individuals # 6: 34-160, and # 12: 52-93, respectively (reference <20)), seemingly without having a direct relation to the clinical condition.

**Identification of mutations in *CLPB* and mutational spectrum**

For each individual, ES resulted in a list of four to six candidate genes. For individual #6, these encompassed *OBSCN, SCN4A, CEACAM20,* and *CLPB;* and for individual #9: *CLVS2, PDZD7, TMEM63C, COG7, BAHCC1* and *CLPB.* Besides being the only overlapping gene, *CLPB* was considered a candidate gene because of the mitochondrial targeting sequence predicting a mitochondrial localization and the previous association of 3-MGA-uria with mitochondrial dysfunction[11]. We detected two heterozygous variants c.1305_1307delinsCCC (p.Glu435_Gly436delinsAspPro) and c.1937G>T (p.Gly646Val) in the coding region of *CLPB* for individual #6 while both parents were heterozygous for one of the two variant alleles. In individual #9, a homozygous variant c.1772C>T (p.Ala591Val, g.72005169C>T; NM_030813.3) was identified and confirmed to be heterozygous in each of the parents. Given these findings, we performed Sanger sequencing of the entire coding region of *CLPB* in 16 additional subjects that shared phenotypes with our discovery cohort; we identified likely pathogenic *CLPB* mutations in 12 of them, all of which segregated (wherever testing was possible) with the disorder under an autosomal recessive paradigm.

In total, we identified 14 different *CLPB* mutations (two nonsense, one frameshift, 11 missense, **Table 2, Figure 3, Figure S3**) in 14 affected individuals from nine independent families of primarily northern European descent (Canada, Australia, Germany, Turkey, Italy, Poland, Estonia). Consistent with a disease-causal role, all variants are either absent or were rare (<0.1% MAF) in the in-house database of 5036 exomes (Dept of Human Genetics, Helmholtz Zentrum, Munich, Germany) and in public databases. The most frequent change c.1222A>G (p.Arg408Gly) had a MAF of 0.011% in the ExAC browser (detected in 22/122,848 alleles, seen only in heterozygosity and never in homozygosity). The nonsense and frameshift mutations are predicted to result in nonsense-mediated mRNA decay (NMD). Of note, each of the most severely affected individuals (#13 and 14) is compound heterozygous for a nonsense and a missense mutation. Since the parents are unavailable for further research, we could not determine whether these nonsense mutations map on the same

haplotype. However, it is tempting to speculate that compound heterozygous nonsense mutations result in a more severe phenotype than missense variants. All missense mutations affect amino acids that are evolutionary conserved across vertebrates and mostly in bacteria **(Figure S4)**. Moreover, all missense mutations are predicted to have a deleterious impact on protein function by different prediction programs (SIFT, Polyphen, mutation taster)[12-14] and map to functional domains and the C-tail of CLPB. There was no clear correlation between the severity of the disease and the position and nature of the specific missense mutations. *CLPB* was shown to be expressed in a broad range of human fetal and adult tissues with a significantly higher expression in adult brain tissues **(Figure S5).** Of note, the expression in fetal brain is approximately five times lower than in adult brain; we also observed low expression in granulocytes.

**Evaluation of mitochondrial function in fibroblasts from affected individuals**

The first 92 amino acid residues of human CLPB are predicted to encode a mitochondrial targeting sequence (MITOPROT: http://ihg.gsf.de/ihg/mitoprot.html)[15]. The predicted mitochondrial localization for human CLPB was confirmed by immunofluorescence of CLPB in U2OS cells **(Figure S6).** Given that other IEMs with 3-MGA-uria as a discriminative feature exhibit mitochondrial dysfunction (e.g. Barth, Sengers, and MEGDEL syndromes), we wondered whether mutations in *CLPB* could affect oxidative phosphorylation[3; 11]. We did not detect histological abnormalities, with the exception of a modest dominance of type I fibers, in muscle of individuals #6 and 9. Evaluation of the oxidative phosphorylation in the same individuals in fresh muscle and cultured fibroblasts did not show any abnormalities**(Table S3)**. Finally, autophagy and mitophagy were assessed in cell lines from four individuals yielding results that were indistinguishable from controls cells **(Figure S7).** Taken together, these data suggest that *CLPB* mutations are unlikely to affect mitochondrial function in general, or respiratory chain oxidative phosphorylation defects or other dysfunction in particular.

**Evaluation of phospholipid metabolism**

Several of the IEM with 3-MGA-uria as discriminative feature have been associated with defective phospholipid metabolism. For instance, typical abnormalities in the quantity and acyl-chain composition of cardiolipin (CL), phosphatidylglycerol (PG) and bis(monoacylglycerol)phosphate (BMP) species are characteristic biomarkers in fibroblasts from individuals with Barth and MEGDEL syndromes[4; 7]. As such, we investigated the

different phospholipid species in fibroblasts from our cohort (**Supplementary methods)**. Phospholipid analysis of fibroblasts of individuals #1, 3, 6, 9 showed normal quantity and acyl-chain composition of PG and BMP compared to seven control cell lines **(Figure S8).** The total amount of CL was lower in affected individuals than in controls (**Figure S8**). However, the significance level ($p = 0.037$) as well as the difference in total CL amounts was marginal, which might reflect the limited number of data points. No abnormalities were observed in other phospholipid species in the fibroblasts from the four individuals tested (phosphatidic acids, phosphatidylcholines, phosphatidylethanolamines, phosphatidylserines, phosphatidylinositols, cardiolipins, sphingomyelines and their lyso-analogues, data not shown). Taken together, we found no unambiguous evidence for a general role of CLPB in phospholipid metabolism.

**Functional analysis of non-synonymous variants in *CLPB* by *in vivo* complementation in zebrafish embryos**

To investigate the pathogenic potential of the non-synonymous missense *CLPB* alleles identified in our study cohort, we turned to the developing zebrafish as a surrogate model. We first evaluated the effect of the MO-induced knockdown on the cerebellar integrity and the ability of human *CLPB* mRNA to rescue that phenotype in the developing embryos. Previous studies have demonstrated that cerebellar defects can be modeled in the developing *D. rerio* [9; 16]. For the present study, we first identified the sole ortholog of *CLPB* in the zebrafish genome by reciprocal BLAST, against which we designed a translational blocking morpholino (tbMO; it was not possible to find a suitable design to block splicing). Injection of 2.5ng of the *clpb* MO resulted in approximately 50% of the injected embryos developing cerebellar defects that ranged in severity from depletion of the axonal connections across the midline of the cerebellum to complete atrophy **(Figure 4 and S9).** The MO-induced phenotype was rescued significantly and reproducibly ($p<0.0001$; performed in triplicate, scored blind to injection cocktail) by co-injection with 200pg of human capped *CLPB* mRNA **(Figure 4 and S9).** By contrast, co-injection of the *clpb* MO with human mRNA bearing each of the four candidate pathogenic alleles tested (p.Arg408Gly, p.Met411Ile, p.Tyr617Cys and p.Gly646Val) were indistinguishable to MO alone [p.Arg408Gly ($p=0.79$), p.Met411Ile ($p=0.54$), p.Tyr617Cys ($p=0.47$) and p.Gly646Val ($p=0.92$)], suggesting that these alleles have little or no residual activity **(Figure 4).**. Overexpression of *CLPB* wt mRNA, or mRNA harbouring each of the four variants had no effect on the cerebellar integrity (**Figure S10**).

**Evaluation of ATPase function of human CLPB**

We were able to express human CLPB in *E.coli* after removing the mitochondrial targeting sequence and confirm that human CLPB retains ATPase activity **(Figure S11)**. Unlike the bacterial ClpB chaperone, the ATPase activity was not found to be stimulated by the presence of casein, a natively unfolded soluble substrate. We also expressed the mutant CLPB_p.Arg408Gly (found in individuals 3,4,5) in *E.coli*. This mutation in the AAA+ domain of CLPB is at the interface between the CLPB oligomers and in the vicinity of the ATP binding site and hence is predicted to influence the ATPase activity through impaired ATP binding. Consistent with this prediction, the ATPase activity level of the mutant protein is 26% of that of wildtype human CLPB in *E. coli* **(Figure S11)**.

**Protein interaction network for CLPB and HAX1**

A database search **(supplementary methods)** resulted in 17 proteins with an established physical interaction with CLPB. The live-cell screen of CLPB against a library of 100 proteins by means of bioluminescence resonance energy transfer (BRET) identified 19 additional direct interactions **(Table S4 and S5**). For HAX1, a total of 38 protein interactions was listed in the BioGRID database. Within the networks of first order protein interactions for both proteins, a link between CLPB and HAX1 is established by mutual interaction with the sarco/endoplasmic reticulum $Ca^{2+}$-ATPase ATP2A2.

**Discussion**

Here we present our clinical and molecular genetic analyses of a cohort of individuals the phenotype(s) of which cannot be reconciled with any known clinical entity. The phenotypic spectrum encompasses ID, congenital neutropenia, progressive brain atrophy, movement disorder and bilateral cataracts. Though all individuals share 3-MGA-uria as a characteristic biomarker, the severity of the other signs and symptoms described shows inter-individual variability that cannot be easily reconciled with allelism at a single causal locus. On aggregate, however, we propose that our cohort represents a distinct clinical entity that leads to an encephalopathy predominantly involving grey matter, which can start as early as in fetal life, as well as chronic moderate to severe neutropenia due to a maturation arrest at the promyelocyte stage. We do not know whether these pathologies are related. However, we note that individuals with the more attenuated neurological phenotypes also had the more severe hematologic disease, which proceeded to leukemia in two siblings.

Under the hypothesis that the consistently observed metabolic signature underpins a discrete molecular genetic disorder, we performed ES in two unrelated individuals, followed by subsequent candidate gene testing in a further 16 affected individuals. Through these studies we identified 14 independent mutations in *CLPB* in 14 individuals from nine unrelated families. Taken together, our data suggest that *CLPB* is the major locus for this phenotype, although additional genes are likely to exist in our *CLPB* mutation-negative families. We further supported these claims by developing a zebrafish model of the disorder, in which we recapitulated key aspects of the neuroanatomical phenotypes of the individuals. Specifically, embryos bereft of endogenous *clpb* show microcephaly, reduction of the size of the optic tectum (OT; a structure equivalent to the superior culicullus in humans), and degeneration of the axons forming the cerebellum, reminiscent of the clinical features in the individuals with *CLPB* mutations. Additionally, co-injection of the *clpb* MO with human mRNA bearing each of the four detected in our cohort alleles tested were indistinguishable to MO alone, suggesting that these alleles have little or no residual activity and the observed syndromic phenotypes in humans are driven by null or near-null mutations in all cases studied. It will be important to accumulate additional individuals with *CLPB* mutations and ascertain whether mutations that retain partial protein function correlate with an attenuated phenotype, or indeed any phenotype at all, since we do not know the tolerance of this biological system for dysfunction.

CLPB belongs to the large AAA+-superfamily (AAA+ = ATP-ases Associated with diverse cellular Activities). AAA+ proteins usually form ring-shaped homo-hexamers [17].

Members of this superfamily typically have one or two highly conserved ATPase domains and are involved in various processes, such as DNA replication and repair, protein disaggregation and refolding and operate as part of dynein motors, as chelatases or proteases [18]. The unifying characteristic of this family of proteins, consist in the hydrolysis of ATP through the AAA+ domain to produce the energy required to exert mechanic force onto their substrates. The human CLPB protein is characterized further by the presence of a specific C-terminal D2 domain (PFAM identifier PF10431), which is typical for AAA+ proteins involved in polypeptide chain threading through the hexamer central channel. Proteins with this C-terminal D2 domain form the subfamily of Caseinolytic peptidase (Clp) proteins, also called HSP100 (Heat shock proteins 100 kDa) [19]. The human CLPB protein was named after its high homology to the C-terminal part of bacterial ClpB protein which is, in co-operation with Hsp70, involved in the process of disaggregation of protein aggregates and hence is called a disaggregase. Bacterial ClpB proteins dissolve protein aggregates and rescue aggregated proteins by assisting them to fold back into a native, biologically active form [20]. What distinguishes the human CLPB protein from its microbial- and plant paralogs is primarily the domain composition. These microbial othologs contain an additional AAA+ domain and a small N-terminal domain (Figure 3) and have an "M-domain", necessary for disaggregation. Another feature characteristic of the human CLPB is the presence of ankyrin repeats instead of the first of two ATPase domains found in bacteria and fungi, which are used commonly as protein–protein interaction platforms (Figure 3) [21; 22]. The species-specific presence of the ankyrin repeats in the N-terminal part of the human protein may have evolved to ensure a more elaborate or more refined substrate recognition, mediate the interaction with as yet unknown protein partners, or even support a putative chaperone function. Despite the fact that only one of the two ATPase domains is retained in the human CLPB, its presence is postulated to be sufficient to mediate the use ATP hydrolysis energy for threading unfolded polypeptide through the central channel of the hexamer ring[23].

Consistent with this hypothsis, we were able to confirm *in vitro* the ATPase activity of human CLPB. Furthermore, we were able to show that upon the presence of the p.Arg408Gly variant (detected in individuals #3,4,5) that is predicted to affect the ATP binding capability of human CLPB, the ATPase activity measured was indeed diminished. Despite the convergence of human and bacterial CLPB proteins on several aspects of molecular function, we found that unlike the bacterial counterpart, the human CLPB cannot be stimulated by casein.

Comparison of the clinical and genetic pathology of individuals with *CLPB* mutations is likewise informative. Mutations in *CLPB* lead to a congenital neutropenia

syndrome comparable to Kostmann disease, driven by mutations in *HAX1* which encodes HCLS1-associated protein X-1 (HAX1)[24]. Both disorders show neurological involvement, which seems, however, to be more severe in individuals with *CLPB* mutations. In individuals with *HAX1* mutations, neurological involvement (epilepsy, ID) can be appreciated only when both *HAX1* isoforms A and B are affected [25]. Despite the variability of neurological symptoms in the two syndromes, remarkable mimicry exists from a haematological standpoint, with individuals affected by either one of the two disorders displaying maturation arrest of the neutrophils a at the promyelocyte stage upon bone marrow examination [26]. Furthermore, individuals with either *CLPB* or *HAX1* mutations also exhibit disease progression from neutropenia into leukemic pictures in the absence of GCSF [27].

On the molecular level, biochemical analyses have established a role of HAX1 in stabilizing the mitochondrial membrane potential and preventing apoptosis in lymphocytes and neurons [24]. These functions of HAX1 can only be exerted when the protein interacts with the mitochondrial proteases presenilin-associated rhomboid-like (PARL) and HtrA serine peptidase 2 (HTRA2); a finding observed in mouse lymphocytes, where the presence of processed HtrA2 prevented the accumulation of mitochondrial outer membrane-associated activated BCL2-associated X protein (Bax), an event that initiates apoptosis[28; 29]. Further evidence for an anti-apoptotic role of HAX1 stems from the observation that it interacts with and downregulates the protein level of ATPase $Ca^{2++}$ transporting cardiac muscle slow twitch 2 (ATP2A2), which regulates the endoplasmic reticulum $Ca^{2+}$-concentration[30]. Evaluation of the protein interaction networks of CLPB predict a biochemical interaction between CLPB and ATP2A2 **(Supplementary methods, Figure 5)**, which allows us to speculate that the effect *of* CLPB mutations on hematopoesis, could be driven by excessive apoptosis, as is the case in Kostmann syndrome.

To enrich our understanding of the CLPB-mutation mediated disease pathomechanisms, we reasoned that CLPB defects might have an effect on lipid biosynthesis and metabolism, similar to what is observed in Barth syndrome, one of the IEM with 3-MGA-uria as discriminative feature, characterized by neutropenia as well as (cardio)myopathy and delayed motor milestones [31]. Despite extensive analysis of the levels of various phospholipids, we detected no involvement of lipid biosynthesis, turnaround and metabolism in the pathogenesis mediated by mutations in *CLPB.* We also were unable to detect overt abnormalities in mitophagy or autophagy in cells from individuals with *CLPB* mutations. In aggregate, our data argue that despite the clinical mimicry between CLPB disease and Barth

syndrome or other IEMs with 3-MGA-uria as a discriminative feature, the mechanisms underlying each condition are diverse.

In conclusion, we describe a new IEM with 3-MGA-uria as discriminative feature (CLPB defect). Underlying mutations were found in *CLPB* and lead to a broad phenotypic spectrum encompassing ID, congenital neutropenia, progressive brain atrophy, movement disorder and bilateral cataracts. The function of human CLPB is currently poorly described but our data show that it might be related to apoptosis.

**Acknowledgements**

We thank the individuals and their parents for participation in this study. The study was financially supported by *Van Leersumfonds, Koninklijke Nederlandse Akademie van Wetenschappen* (project VLF2013277 to SW), by the Dutch society for the study of inborn errors of metabolism *(ESN stimulatie beurs* to SW), by the NARSAD Young Investigator Grant from BBRF (to CG) and by NIH P50MH094268 (to NK). NK is a Distinguished George W. Brumley Professor. CK is the recipient of a career development award from the Hermann and Lilly Schilling Foundation and is supported by a grant from the *Deutsche Forschungsgemeinschaft* (DFG). We thank Edwin van Kaauwen and Liesbeth Wintjes, Translational Metabolic Laboratory, Department of Laboratory Medicine, RadboudUMC Nijmegen, The Netherlands for excellent technical assistance. We thank Dirk Klee, Department of Diagnostic and Interventional Radiology, Heinrich-Heine University, Düsseldorf, Germany for helping to select the MRI images of individual 8. We thank Han Brunner, Institute of Human Genetics, RadboudUMC Nijmegen; K. Liberek, Department of Molecular and Cellular Biology, Intercollegiate Faculty of Biotechnology, University of Gdańsk, Poland; Angela Luyf and Antione van Kampen, Bioinformatics Laboratory, Department of Clinical Epidemiology, Biostatistics and Bioinformatics, AMC, Amsterdam and Mathias Woidy and Philipp Guder, Department of Molecular Pediatrics, Dr. von Hauner Children's Hospital, Ludwig-Maximilians-University, Munich, Germany as well as Harry Kampinga ,University Medical Center Groningen, Department of Cell Biology, Groningen, for fruitful discussion.

All authors declare no competing financial interests.

**WEB RESOURCES**

The URLs for data presented herein are as follows:

Exome Aggregation Consortium , Cambridge, MA (ExAC, http://exac.broadinstitute.org); NHLBI Exome Sequencing Project Exome Variant Server (http://evs.gs.washington.edu/EVS/); Online Mendelian Inheritance in Man (OMIM, http://www.omim.org); Biological General Repository for Interaction Datasets (BioGRID, http://thebiogrid.org/); Human Protein Reference Database (HPRD, http://www.hsls.pitt.edu/obrc/index.php?page=URL1055173331); Molecular Interactions Database (MINT, http://databib.org/repository/602); Search Tool for the Retrieval of Interacting Genes/Proteins (STRING, http://string-db.org/)

## References


1. de Ligt, J., Willemsen, M.H., van Bon, B.W., Kleefstra, T., Yntema, H.G., Kroes, T., Vulto-van Silfhout, A.T., Koolen, D.A., de Vries, P., Gilissen, C., et al. (2012). Diagnostic exome sequencing in persons with severe intellectual disability. The New England journal of medicine 367, 1921-1929.
2. Gilissen, C., Hehir-Kwa, J.Y., Thung, D.T., van de Vorst, M., van Bon, B.W., Willemsen, M.H., Kwint, M., Janssen, I.M., Hoischen, A., Schenck, A., et al. (2014). Genome sequencing identifies major causes of severe intellectual disability. Nature 511, 344-347.
3. Wortmann, S.B., Duran, M., Anikster, Y., Barth, P.G., Sperl, W., Zschocke, J., Morava, E., and Wevers, R.A. (2013). Inborn errors of metabolism with 3-methylglutaconic aciduria as discriminative feature: proper classification and nomenclature. Journal of inherited metabolic disease 36, 923-928.
4. Wortmann, S.B., Espeel, M., Almeida, L., Reimer, A., Bosboom, D., Roels, F., de Brouwer, A.P., and Wevers, R.A. (2014). Inborn errors of metabolism in the biosynthesis and remodelling of phospholipids. Journal of inherited metabolic disease.
5. Donadieu, J., Fenneteau, O., Beaupain, B., Mahlaoui, N., and Chantelot, C.B. (2011). Congenital neutropenia: diagnosis, molecular bases and patient management. Orphanet journal of rare diseases 6, 26.
6. Haack, T.B., Gorza, M., Danhauser, K., Mayr, J.A., Haberberger, B., Wieland, T., Kremer, L., Strecker, V., Graf, E., Memari, Y., et al. (2014). Phenotypic spectrum of eleven patients and five novel MTFMT mutations identified by exome sequencing and candidate gene screening. Molecular genetics and metabolism 111, 342-352.
7. Wortmann, S.B., Vaz, F.M., Gardeitchik, T., Vissers, L.E., Renkema, G.H., Schuurs-Hoeijmakers, J.H., Kulik, W., Lammens, M., Christin, C., Kluijtmans, L.A., et al. (2012). Mutations in the phospholipid remodeling gene SERAC1 impair mitochondrial function and intracellular cholesterol trafficking and cause dystonia and deafness. Nature genetics 44, 797-802.
8. Niederriter, A.R., Davis, E.E., Golzio, C., Oh, E.C., Tsai, I.C., and Katsanis, N. (2013). In vivo modeling of the morbid human genome using Danio rerio. Journal of visualized experiments : JoVE, e50338.
9. Margolin, D.H., Kousi, M., Chan, Y.M., Lim, E.T., Schmahmann, J.D., Hadjivassiliou, M., Hall, J.E., Adam, I., Dwyer, A., Plummer, L., et al. (2013). Ataxia, dementia, and hypogonadotropism caused by disordered ubiquitination. The New England journal of medicine 368, 1992-2003.
10. Norby, J.G. (1988). Coupled assay of Na+,K+-ATPase activity. Methods in enzymology 156, 116-119.
11. Wortmann, S.B., Kluijtmans, L.A., Rodenburg, R.J., Sass, J.O., Nouws, J., van Kaauwen, E.P., Kleefstra, T., Tranebjaerg, L., de Vries, M.C., Isohanni, P., et al. (2013). 3-Methylglutaconic aciduria--lessons from 50 genes and 977 patients. Journal of inherited metabolic disease 36, 913-921.
12. Ng, P.C., and Henikoff, S. (2003). SIFT: Predicting amino acid changes that affect protein function. Nucleic acids research 31, 3812-3814.
13. Adzhubei, I.A., Schmidt, S., Peshkin, L., Ramensky, V.E., Gerasimova, A., Bork, P., Kondrashov, A.S., and Sunyaev, S.R. (2010). A method and server for predicting damaging missense mutations. Nature methods 7, 248-249.
14. Schwarz, J.M., Rodelsperger, C., Schuelke, M., and Seelow, D. (2010). MutationTaster evaluates disease-causing potential of sequence alterations. Nature methods 7, 575-576.
15. Claros, M.G., and Vincens, P. (1996). Computational method to predict mitochondrially imported proteins and their targeting sequences. European journal of biochemistry / FEBS 241, 779-786.
16. Matsui, H., Namikawa, K., Babaryka, A., and Koster, R.W. (2014). Functional regionalization of the teleost cerebellum analyzed in vivo. Proceedings of the National Academy of Sciences of the United States of America 111, 11846-11851.

17. Neuwald, A.F., Aravind, L., Spouge, J.L., and Koonin, E.V. (1999). AAA+: A class of chaperone-like ATPases associated with the assembly, operation, and disassembly of protein complexes. Genome research 9, 27-43.
18. Snider, J., Thibault, G., and Houry, W.A. (2008). The AAA+ superfamily of functionally diverse proteins. Genome biology 9, 216.
19. Zolkiewski, M. (2006). A camel passes through the eye of a needle: protein unfolding activity of Clp ATPases. Molecular microbiology 61, 1094-1100.
20. Rosenzweig, R., Moradi, S., Zarrine-Afsar, A., Glover, J.R., and Kay, L.E. (2013). Unraveling the mechanism of protein disaggregation through a ClpB-DnaK interaction. Science 339, 1080-1083.
21. Mosavi, L.K., Cammett, T.J., Desrosiers, D.C., and Peng, Z.Y. (2004). The ankyrin repeat as molecular architecture for protein recognition. Protein science : a publication of the Protein Society 13, 1435-1448.
22. Li, J., Mahajan, A., and Tsai, M.D. (2006). Ankyrin repeat: a unique motif mediating protein-protein interactions. Biochemistry 45, 15168-15178.
23. Weibezahn, J., Tessarz, P., Schlieker, C., Zahn, R., Maglica, Z., Lee, S., Zentgraf, H., Weber-Ban, E.U., Dougan, D.A., Tsai, F.T., et al. (2004). Thermotolerance requires refolding of aggregated proteins by substrate translocation through the central pore of ClpB. Cell 119, 653-665.
24. Klein, C., Grudzien, M., Appaswamy, G., Germeshausen, M., Sandrock, I., Schaffer, A.A., Rathinam, C., Boztug, K., Schwinzer, B., Rezaei, N., et al. (2007). HAX1 deficiency causes autosomal recessive severe congenital neutropenia (Kostmann disease). Nature genetics 39, 86-92.
25. Germeshausen, M., Grudzien, M., Zeidler, C., Abdollahpour, H., Yetgin, S., Rezaei, N., Ballmaier, M., Grimbacher, B., Welte, K., and Klein, C. (2008). Novel HAX1 mutations in patients with severe congenital neutropenia reveal isoform-dependent genotype-phenotype associations. Blood 111, 4954-4957.
26. Kostmann, R. (1956). Infantile genetic agranulocytosis; agranulocytosis infantilis hereditaria. Acta paediatrica Supplementum 45, 1-78.
27. Yetgin, S., Olcay, L., Koc, A., and Germeshausen, M. (2008). Transformation of severe congenital neutropenia to early acute lymphoblastic leukemia in a patient with HAX1 mutation and without G-CSF administration or receptor mutation. Leukemia 22, 1797.
28. Chao, J.R., Parganas, E., Boyd, K., Hong, C.Y., Opferman, J.T., and Ihle, J.N. (2008). Hax1-mediated processing of HtrA2 by Parl allows survival of lymphocytes and neurons. Nature 452, 98-102.
29. Cilenti, L., Soundarapandian, M.M., Kyriazis, G.A., Stratico, V., Singh, S., Gupta, S., Bonventre, J.V., Alnemri, E.S., and Zervos, A.S. (2004). Regulation of HAX-1 anti-apoptotic protein by Omi/HtrA2 protease during cell death. The Journal of biological chemistry 279, 50295-50301.
30. Vafiadaki, E., Arvanitis, D.A., Pagakis, S.N., Papalouka, V., Sanoudou, D., Kontrogianni-Konstantopoulos, A., and Kranias, E.G. (2009). The anti-apoptotic protein HAX-1 interacts with SERCA2 and regulates its protein levels to promote cell survival. Molecular biology of the cell 20, 306-318.
31. Houtkooper, R.H., Turkenburg, M., Poll-The, B.T., Karall, D., Perez-Cerda, C., Morrone, A., Malvagia, S., Wanders, R.J., Kulik, W., and Vaz, F.M. (2009). The enigmatic role of tafazzin in cardiolipin metabolism. Biochimica et biophysica acta 1788, 2003-2014.
32. Leidhold, C., von Janowsky, B., Becker, D., Bender, T., and Voos, W. (2006). Structure and function of Hsp78, the mitochondrial ClpB homolog. Journal of structural biology 156, 149-164.
33. Letunic, I., Doerks, T., and Bork, P. (2014). SMART: recent updates, new developments and status in 2015. Nucleic acids research.
34. Sedgwick, S.G., and Smerdon, S.J. (1999). The ankyrin repeat: a diversity of interactions on a common structural framework. Trends in biochemical sciences 24, 311-316.
35. Rodenburg, R.J. (2011). Biochemical diagnosis of mitochondrial disorders. Journal of inherited metabolic disease 34, 283-292.

36. Rakovic, A., Grunewald, A., Kottwitz, J., Bruggemann, N., Pramstaller, P.P., Lohmann, K., and Klein, C. (2011). Mutations in PINK1 and Parkin impair ubiquitination of Mitofusins in human fibroblasts. PloS one 6, e16746.
37. Houtkooper, R.H., Rodenburg, R.J., Thiels, C., van Lenthe, H., Stet, F., Poll-The, B.T., Stone, J.E., Steward, C.G., Wanders, R.J., Smeitink, J., et al. (2009). Cardiolipin and monolysocardiolipin analysis in fibroblasts, lymphocytes, and tissues using high-performance liquid chromatography-mass spectrometry as a diagnostic test for Barth syndrome. Analytical biochemistry 387, 230-237.
38. Bakele, M., Lotz-Havla, A.S., Jakowetz, A., Carevic, M., Marco, V., Munta, A.C., Gerstin, S.W., and Hartl, D. (2014). An interactive network of elastase, secretases, and PAR-2 protein regulates CXCR1 receptor surface expression on neutrophils. The Journal of biological chemistry 289, 20516-20525.
39. Gersting, S.W., Lotz-Havla, A.S., and Muntau, A.C. (2012). Bioluminescence resonance energy transfer: an emerging tool for the detection of protein-protein interaction in living cells. Methods in molecular biology (Clifton, NJ) 815, 253-263.
40. Braun, P., Tasan, M., Dreze, M., Barrios-Rodiles, M., Lemmens, I., Yu, H., Sahalie, J.M., Murray, R.R., Roncari, L., de Smet, A.S., et al. (2009). An experimentally derived confidence score for binary protein-protein interactions. Nature methods 6, 91-97.
41. Sowa, M.E., Bennett, E.J., Gygi, S.P., and Harper, J.W. (2009). Defining the human deubiquitinating enzyme interaction landscape. Cell 138, 389-403.
42. Bennett, E.J., Rush, J., Gygi, S.P., and Harper, J.W. (2010). Dynamics of cullin-RING ubiquitin ligase network revealed by systematic quantitative proteomics. Cell 143, 951-965.
43. Joshi, P., Greco, T.M., Guise, A.J., Luo, Y., Yu, F., Nesvizhskii, A.I., and Cristea, I.M. (2013). The functional interactome landscape of the human histone deacetylase family. Molecular systems biology 9, 672.
44. Taipale, M., Tucker, G., Peng, J., Krykbaeva, I., Lin, Z.Y., Larsen, B., Choi, H., Berger, B., Gingras, A.C., and Lindquist, S. (2014). A quantitative chaperone interaction network reveals the architecture of cellular protein homeostasis pathways. Cell 158, 434-448.
45. Venkatesan, K., Rual, J.F., Vazquez, A., Stelzl, U., Lemmens, I., Hirozane-Kishikawa, T., Hao, T., Zenkner, M., Xin, X., Goh, K.I., et al. (2009). An empirical framework for binary interactome mapping. Nature methods 6, 83-90.
46. Colland, F., Jacq, X., Trouplin, V., Mougin, C., Groizeleau, C., Hamburger, A., Meil, A., Wojcik, J., Legrain, P., and Gauthier, J.M. (2004). Functional proteomics mapping of a human signaling pathway. Genome research 14, 1324-1332.
47. Giannone, R.J., McDonald, H.W., Hurst, G.B., Shen, R.F., Wang, Y., and Liu, Y. (2010). The protein network surrounding the human telomere repeat binding factors TRF1, TRF2, and POT1. PloS one 5, e12407.
48. Leonard, D., Ajuh, P., Lamond, A.I., and Legerski, R.J. (2003). hLodestar/HuF2 interacts with CDC5L and is involved in pre-mRNA splicing. Biochemical and biophysical research communications 308, 793-801.
49. Stes, E., Laga, M., Walton, A., Samyn, N., Timmerman, E., De Smet, I., Goormachtig, S., and Gevaert, K. (2014). A COFRADIC protocol to study protein ubiquitination. Journal of proteome research 13, 3107-3113.
50. Holzmann, J., Frank, P., Loffler, E., Bennett, K.L., Gerner, C., and Rossmanith, W. (2008). RNase P without RNA: identification and functional reconstitution of the human mitochondrial tRNA processing enzyme. Cell 135, 462-474.
51. Behrends, C., Sowa, M.E., Gygi, S.P., and Harper, J.W. (2010). Network organization of the human autophagy system. Nature 466, 68-76.
52. Biasini, M., Bienert, S., Waterhouse, A., Arnold, K., Studer, G., Schmidt, T., Kiefer, F., Cassarino, T.G., Bertoni, M., Bordoli, L., et al. (2014). SWISS-MODEL: modelling protein tertiary and quaternary structure using evolutionary information. Nucleic acids research 42, W252-258.
53. Lee, S., Sowa, M.E., Watanabe, Y.H., Sigler, P.B., Chiu, W., Yoshida, M., and Tsai, F.T. (2003). The structure of ClpB: a molecular chaperone that rescues proteins from an aggregated state. Cell 115, 229-240.

54. Mogk, A., Schlieker, C., Strub, C., Rist, W., Weibezahn, J., and Bukau, B. (2003). Roles of individual domains and conserved motifs of the AAA+ chaperone ClpB in oligomerization, ATP hydrolysis, and chaperone activity. The Journal of biological chemistry 278, 17615-17624.
55. Biter, A.B., Lee, S., Sung, N., and Tsai, F.T. (2012). Structural basis for intersubunit signaling in a protein disaggregating machine. Proceedings of the National Academy of Sciences of the United States of America 109, 12515-12520.
56. Pfaffl, M.W. (2001). A new mathematical model for relative quantification in real-time RT-PCR. Nucleic acids research 29, e45.
57. Livak, K.J., and Schmittgen, T.D. (2001). Analysis of relative gene expression data using real-time quantitative PCR and the 2(-Delta Delta C(T)) Method. Methods (San Diego, Calif) 25, 402-408.

**Tables and figures**

Table 1. Clinical, biochemical and neuroradiological findings in individuals with mutations in *CLPB*

| Individual, gender | Family | ID | Mutation (aa) | Neutropenia | Generalized brain atrophy | Movement disorder | Muscle tone | cataracts | 3-MGA-uria | Current age | other |
|---|---|---|---|---|---|---|---|---|---|---|---|
| 1, m | 1 | no | | CS | NA | - | normal | - | + | 10 y | |
| 2, f | 1 | no | p.Met411Ile/ p.Tyr617Cys | CM | no | - | normal | + | + | 8y | |
| 3, m | 2 | moderate | p.Arg408Gly/ p.Arg417* | IS | NA | ataxia, dyspraxia | floppy infant, mild truncal hypotonia | - | + | 5 9/12 y | IUGR, neonatal hypoglycaemia, microcephaly |
| 4, f | 3 | moderate | p.Arg408Gly/ p.Arg417* | - | NA | - | floppy infant, mild truncal hypotonia | - | + | 2 2/12 y | IUGR, neonatal hypoglycaemia, microcephaly |
| 5, m | 3 | moderate | p.Arg408Gly/ p.Arg417* | - | NA | - | floppy infant, mild truncal hypotonia | - | + | 2 2/12 y | IUGR, neonatal hypoglycaemia, microcephaly |
| 6, f | 4 | mild | p.Glu435_Gly436delinsAspPro/ p.Gly646Val | CM | + | ataxia, dysarthria, tremor | mild tetraspasticity | + | + | 18 y | microcephaly, hypothyreoidea, hypergonadotropic hypogonadism |
| 7, f | 5 | severe | p.Cys486Arg homo | - | + | dystonia | floppy infant, progressive tetraspasticity | + | + | 17 y | microcephaly IUGR, epilepsy, hypothyreoidea, mild cardiac septal hypertrophy, nystagmus |
| 8, f | 5 | severe | p.Cys486Arg homo | - | + | dystonia, athetosis | floppy infant, progressive tetraspasticity | - | + | 9 y | microcephaly, epilepsy, nystagmus |

| | | | | | | | | | | | |
|---|---|---|---|---|---|---|---|---|---|---|---|
| 9, f | 6 | severe | p.Ala591Val homo | CS | +* | hyperkinesia, dystonia | floppy infant, progressive tetraspasticity | + | + | 3 10/12 y** | microcephaly, IUGR, neonatal hypoglycaemia, life-threatening drooling |
| 10, m | 7 | severe | p.Tyr272Cys/ p.Tyr567Cys | CS | + | - | floppy infant, progressive tetraspasticity | NA | NA | 3 m** | hepatosplenomegaly, leukemia, facial dysmorphism |
| 11, f | 7 | severe | p.Tyr272Cys/ p.Tyr567Cys | CS | + | - | floppy infant, generalized hypotonia | NA | + | 3 m** | hepatosplenomegaly, myelodysplastic and preleukemic syndrome, facial dysmorphism |
| 12, f | 8 | severe | p.Cys647Leufs *26/ p.Ile682Asn | CM | + | ataxia, tremor | stiff baby | - | + | 5 m** | Microcephaly, IUGR, epilepsy |
| 13, m | 9 | severe | p.Arg250*/ p.Arg417*/ p.Glu501Lys | CS | NA | jittery | stiff baby | NA | + | 24 d** | epilepsy |
| 14, m | 9 | severe | p.Arg250*/ p.Arg417*/ p.Glu501Lys | CS | NA | NA | stiff baby | NA | NA | 54 d** | IUGR, mild dilated cardiomyopathy |

All individuals are of Caucasian descent. CM = chronic moderate , CS = chronic severe, ID = intellectual disability, IS = intermittent severe. IUGR= intrauterine growth retardation; NA = not available, 3-MGA-uria = 3-methylglutaconic aciduria, *isolated cerebellar atrophy, **age deceased.

Table 2. Mutations in *CLPB* and their predicted effects at the protein level

| Individual | Mutation (nt) | Mutation (aa) | exon | Mutation type | Domains affected | (Predicted) effect | Occurence in the ExAC browser |
|---|---|---|---|---|---|---|---|
| 13,14 | c.748C>T | p.Arg250* | 6 | nonsense | all | Truncated protein, NMD | not detected |
| 10,11 | c.815A>G | p.Tyr272Cys | 6 | missense | ANK | | 2 het / 122918 alleles |
| 3, 4, 5 | c.1222A>G | p.Arg408Gly | 11 | missense | AAA+ | Likely affects ATP binding | 22 het / 122848 alleles |
| 1,2 | c.1233G>A | p.Met411Ile | 11 | missense | AAA+ | Likely affects ATP binding | not detected |
| 3, 4, 5, 13, 14 | c.1249C>T | p.Arg417* | 11 | nonsense | AAA+, D2 | Truncated protein, NMD | 4 het / 122824 alleles |
| 6 | c.1305_1307 delinsCCC | p.Glu435_Gly436 delinsAspPro | 12 | missense | AAA+ | Likely to affect substrate interaction [32] | not detected |
| 7,8 | c.1456T>C | p.Cys486Arg | 13 | missense | AAA+ | | not detected |
| 13,14 | c.1501G>A | p.Glu501Lys | 13 | missense | AAA+ | | 1 het / 121514 alleles |
| 10,11 | c.1700A>G | p.Tyr567Cys | 15 | missense | D2 boundary | | 5 het /122590 alleles |
| 9 | c.1772C>T | p.Ala591Val | 16 | missense | D2 | Likely affects stabilization of D2 domain | not detected |
| 1,2 | c.1850A>G | p.Tyr617Cys | 16 | missense | D2 | Likely affects oligomer stabilization | not detected |
| 6 | c.1937G>T | p.Gly646Val | 17 | missense | D2 | | 1 het / 122598 alleles |
| 12 | c.1937dupG | p.Cys647Leufs*26 | 17 | frameshift | D2 | Truncated protein, NMD | not detected |
| 12 | c.2045T>A | p.Ile682Asn | 17 | missense | C-tail | | not detected |

Overview of all mutations found in *CLPB* in the different individuals; aa = amino acid, het = heterozygous, NMD= nonsense-mediated mRNA decay, nt=nucleotide.

Figure 1

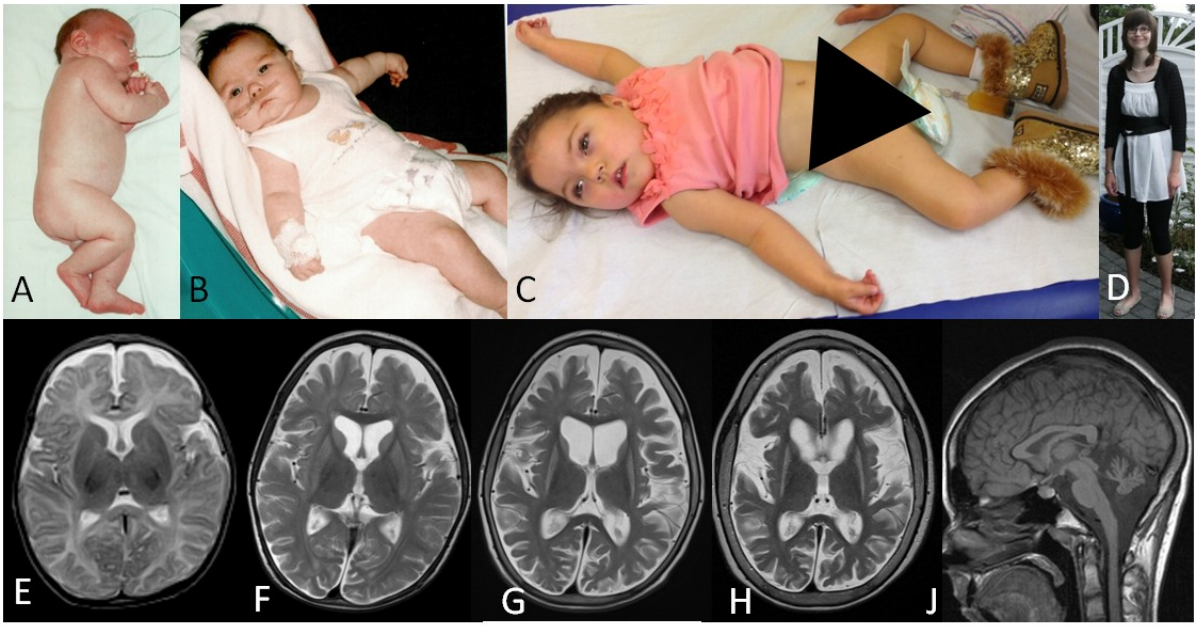


Individual photographs and MRI findings. (A) Individual #10 was born with increased muscle tone. (B) Study participants #11 and (C) #9 with tented mouth, hypertelorism, and truncal hypotonia. (D) Individual #6 displayed no facial dysmorphisms and is able to stand freely. (E-H) Consecutive T2-weighted MR images of individuals #8, axial view, at the age of 2.5 months (E), 16 months (F), 3.5 years (G) and 7 years (H), respectively demonstrating progressive brain atrophy with both cortical and white matter volume decrease over time. Progressive, symmetrical basal ganglia atrophy was supported by abnormally increased T2 signal intensity in the caudate nucleus and putamen starting at the age of 16 months. (J) Isolated cerebellar atrophy was observed in study participant #6 as determined T1-weighted sagittal MRI.

Figure 2

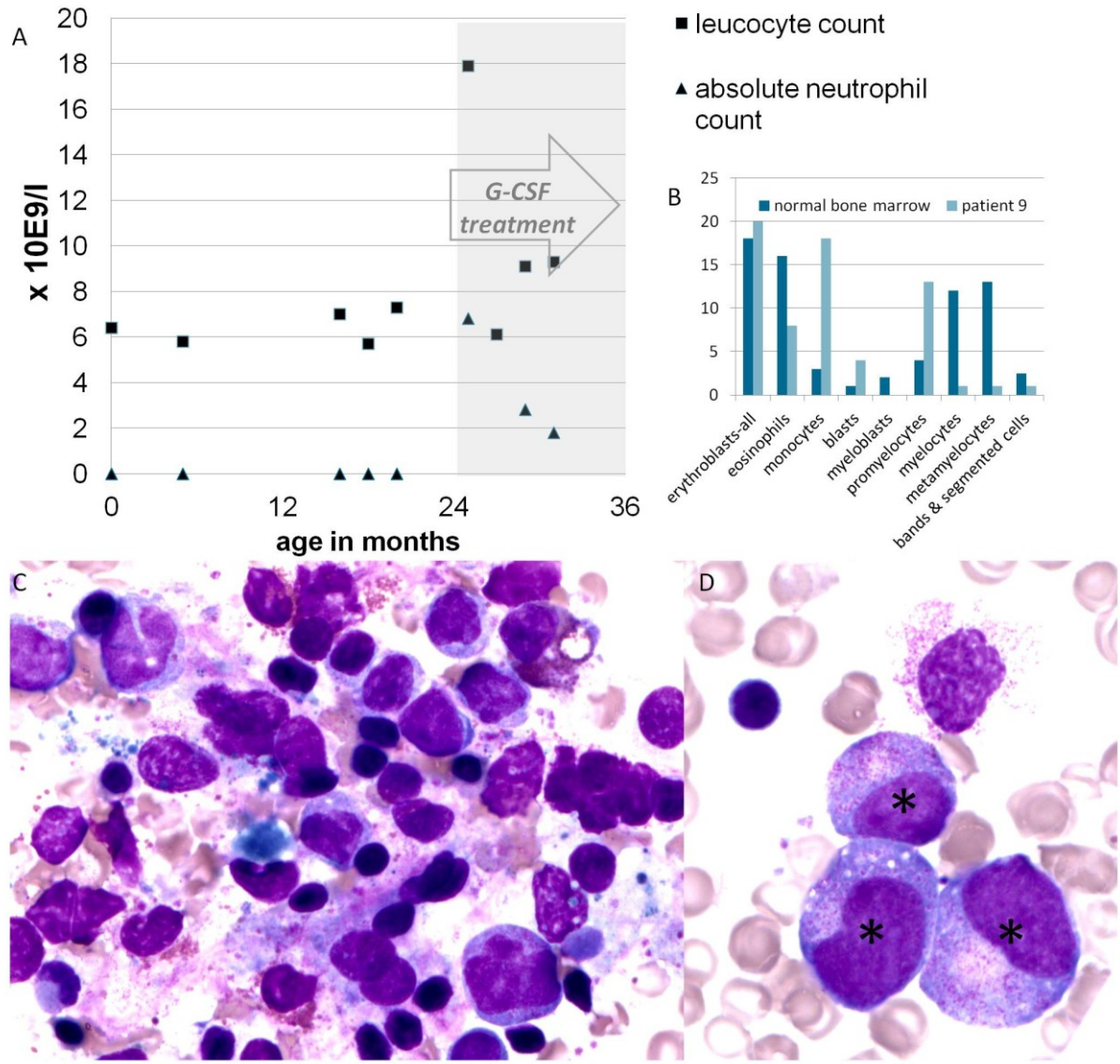


(A) Leucocyte (reference range 4.5 -10 G/L) and absolute neutrophil count (reference range at birth: 12-15 G/L, 2-12 months: >2 G/L, >12 months: > 1.5 G/L) of individual #9 before and during successful treatment with G-CSF. (B) The total bone marrow composition at 20 months of life of the same individual: blasts 4%, promyelocytes 13%, myelocytes 1%, metamyelocytes 1%, bands & segmented cells 1 %, neutrophils 2%, basophils 0%, eosinophils 8%, lymphocytes 32%, monocytes 18%, plasma-cells 0%, normoblasts 20% in comparison with a normal bone marrow. (C, D) Crista biopsy of individual #9 at 20 months of age shown in two distinct magnifications. The bone marrow contains many promyelocytes (*), but no mature neutrophils (maturation arrest at promyelycte stage), many macrophages, hemophagocytosis as well as atypical lymphocytes

Figure 3

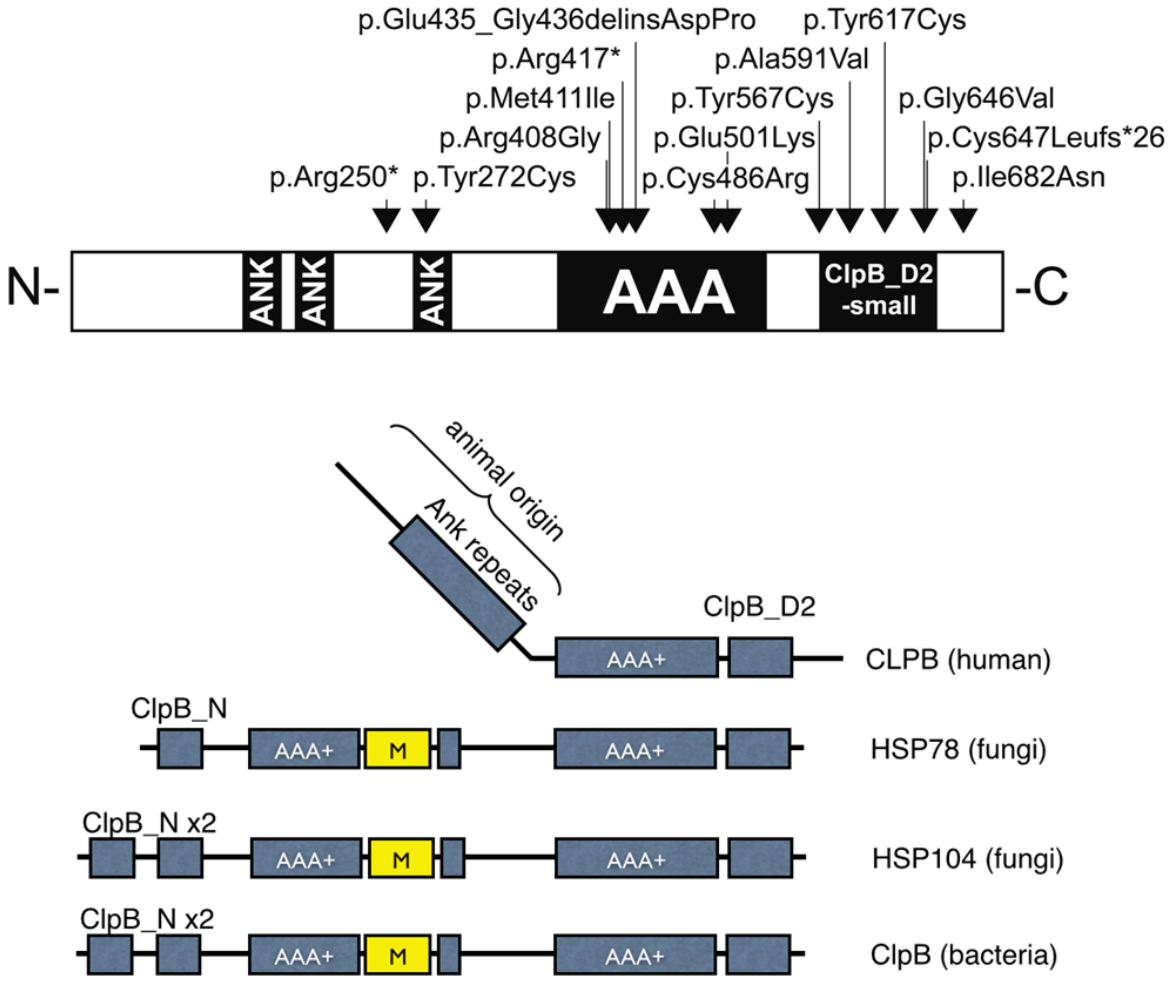


(A) Schematic representation of human CLPB including the positions of all mutations identified. Black boxes represent the two main functional domains: the ankyrin domain (ANK) consisting of a short 34 residue repeat implicated in a wide range of protein-protein interactions and the ATPase domain (AAA+) [33; 34]. (B) Evolutionary changes in domain composition of CLPB proteins in human, fungi (mitochondrial HSP78 and cytosolic HSP104) and bacteria. All CLPB-family homologs possess at least a single AAA+ domain and the specific CLPB-D2 domain. In contrast to human CLPB, fungi and bacteria possess an "M domain", a ClpB N-domain and an additional AAA+ domain. Ankyrin repeats are only present in the human homolog and are likely species-specific.

Figure 4

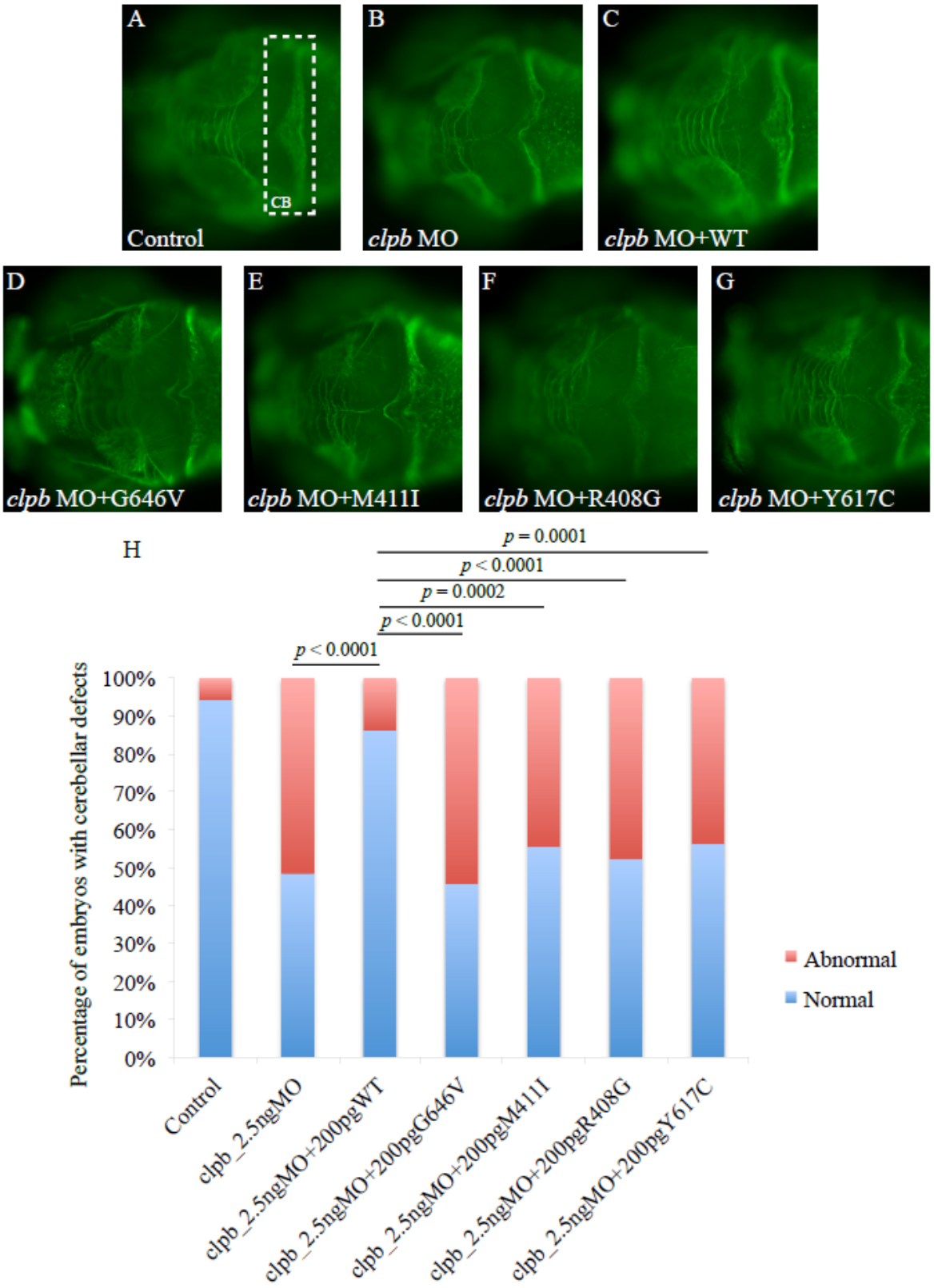
A
CB
Control
B
clpb MO
C
clpb MO+WT
D
clpb MO+G646V
E
clpb MO+M411I
F
clpb MO+R408G
G
clpb MO+Y617C
H
p = 0.0001
p < 0.0001
p = 0.0002
p < 0.0001
p < 0.0001
Percentage of embryos with cerebellar defects
100%
90%
80%
70%
60%
50%
40%
30%
20%
10%
0%
Control
clpb_2.5ngMO
clpb_2.5ngMO+200pgWT
clpb_2.5ngMO+200pgG646V
clpb_2.5ngMO+200pgM411I
clpb_2.5ngMO+200pgR408G
clpb_2.5ngMO+200pgY617C
Abnormal
Normal

*In vivo* complementation of four *CLPB* alleles identified in evaluated study participants, in zebrafish. (A-G) Dorsal view of the developing zebrafish brain stained with acetylated tubulin at 3 days post fertilization (dpf). The cerebellum (CB) is highlighted by a white dashed rectangle in panel A showing a control embryo. (A-C) Control, morpholino injection and rescue by human WT mRNA. (D-G) Illustration of the effects of the tested alleles. (H) Graphic representation of the scoring for CB defects in control and injected embryos. Co-injection of MO with WT human *CLPB* mRNA results is a statistically significant reduction in the number of embryos with cerebellar defects ($p<0.0001$). By contrast, co-injection of MO with each of the human *CLPB* mRNAs carrying the four mutations tested score as pathogenic being indistinguishable from the MO-injected embryos.

**Figure 5**

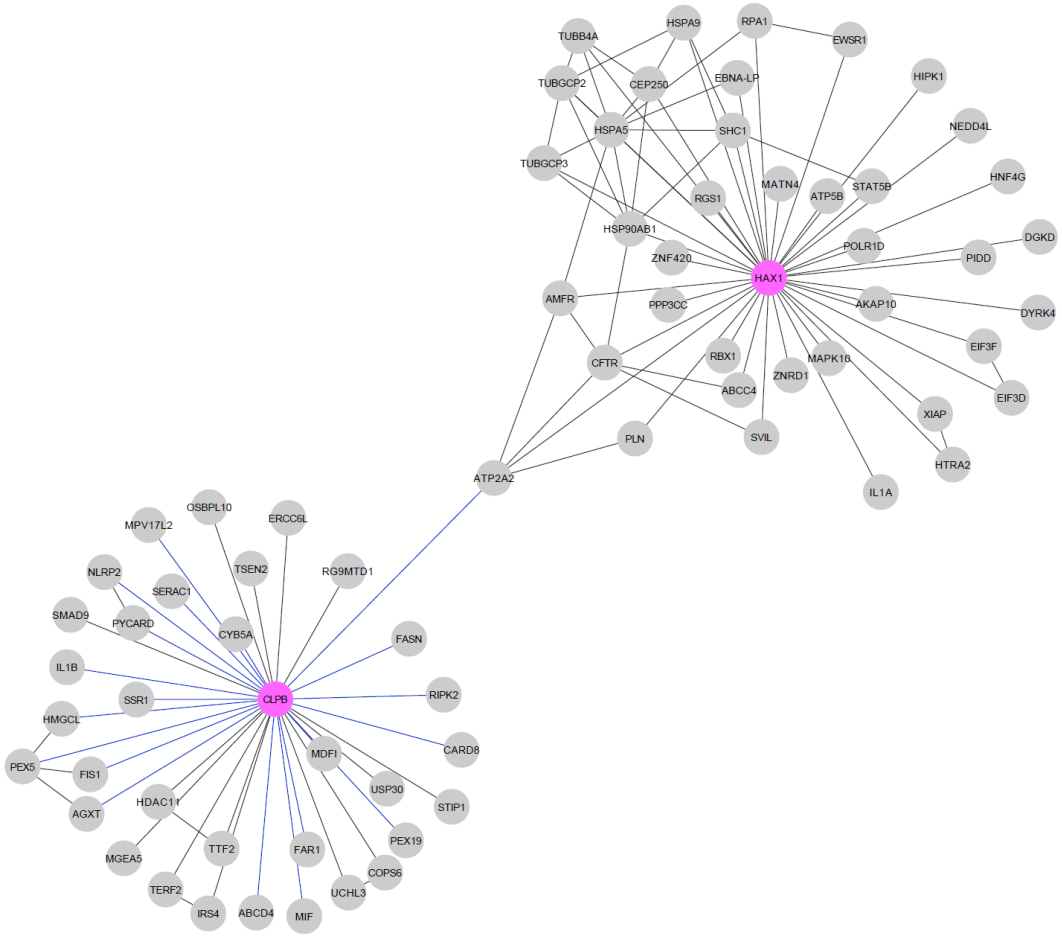


Protein interaction network for CLPB and HAX1. A database search resulted in 17 proteins with an established physical interaction with CLPB. The live-cell screen of CLPB against a library of 100 proteins by means of bioluminescence resonance energy transfer (BRET) identified 19 additional direct interactions **(Table S4 and S5**). For HAX1, a total of 38 protein interactions was listed in the BioGRID database. Within the networks of first order protein interactions for both proteins, a link between CLPB and HAX1 is established by mutual interaction with the sarco/endoplasmic reticulum $Ca^{2+}$-ATPase ATP2A2.

**Supplementary information**

**Supplementary case reports**

**1. Mild phenotype (cataracts, neutropenia, no ID/DD, no movement disorder, no MRI abnormalities)**

**Individual 1** came to medical attention at 18 months of age with fever and skin infection requiring antibiotics. Severe neutropenia (0.1 G/L) was noted. His neutrophil counts varied (0.1 – 1.1. G/L) in the further course, but he never experienced any infections nor required antibiotics since then. When his younger sister, **individual 2,** was born with bilateral nuclear cataracts, and also showed neutropenia (0.7 G/L) both individuals were evaluated further. Their development and growth until the age of 10 and eight years, respectively, is normal. Both recently had an extensive psychological examination including an IQ assessment, which was above average in all dimensions. The brother was further diagnosed with attention deficit hyperactivity disorder (ADHD), dyslexia and dysgraphia and the sister with a tendency to impulsivity. Though no radiological data are available for patient 1, the MRI of individual 2 at the age of eight years was normal.

**2. Moderate phenotype (cataracts, neutropenia, infections, congenital hypotonia progressing to spasticity, mild to severe ID/DD, movement disorder, increasing severity of MRI abnormalities)**

I**ndividual 3** presented with intra-uterine growth restriction (IUGR; birth weight p10, length p50, head circumference p3) and bilateral talipes were noted on prenatal ultrasound. The newborn period was complicated by generalized hypotonia, feeding difficulties, and one episode of hypoglycaemia. He underwent serial casting and an achilles tenotomy for talipes. He has intermittent left esotropia and amblyopia with normal fundi, but no cataracts. Since the age of ten months he had recurrent episodes of neutropenia (0.04 G/L) in the context of febrile illnesses but has responded well to short courses of G-CSF. His development is globally delayed. Currently, at the age of 5 years nine months, he has mild truncal hypotonia, is able to walk independently but with a stooped posture and ataxic gait. He is able to spell his name and speak in simple sentences. He has short stature (p10) and microcephaly (p2). Echocardiography is normal.

The proband has a younger brother, **individual 4,** and sister, **individual 5** (uncomplicated twin pregnancy). The boy had generalized hypotonia, more prominent than his twin sister. Both had problems with hypoglycaemia and poor feeding. At seven months of age, bilateral

cataracts were detected in the male individual, which were removed surgically. Ophthalmological investigations in the girl were normal. At 18 months microcephaly became apparent in both children. Both affected individuals remain hypotonic and although they continue gaining skills, their development is globally delayed. At 21 months of age, they are able to sit independently and to crawl. They babble and are able to indicate what they want. Neither twin has had documented febrile neutropenic episodes to date. Echocardiography, hearing assessment and cranial ultrasound were normal.

**Individual 6** was evaluated for developmental delay and tremor from the age of 17 months onwards. She has bilateral cataracts and chronic moderate neutropenia (0.6-0.9 G/L) but did not suffer recurrent infections beside *Salmonella* infection at 17 years of age. Hypothyroidism and hypergonadotropic hypogonadism were treated with hormonal substitution. She is now 18 years old and finished regular school with some support. Upon neurologic examination she shows normal head circumference, mild bilateral spasticity and severe cerebellar ataxia, dysarthria and tremor. She can walk with assistance and has no swallowing problems. MRI examination showed progressive, isolated, cerebellar atrophy **(Figure 1I ).**

At the age of three months, muscular hypotonia, poor eye contact and uncoordinated eye movements were noted in the female **individual 7**. On eye examination a salt and pepper pigmentation pattern was observed, but no cataracts were observed. At the age of two years swallowing problems necessitated gastrostomy. From the age of four years seizures were noted. Eye-examination at that age was normal apart from strabismus (no cataract, no optic atrophy, no salt and pepper pigmentation). From the age of seven years onwards progressive athetosis and dystonia were noted as well as progressive spasticity of the legs. Serial MRI's up to the age of ten years showed progressive cerebral, cerebellar and basal ganglia atrophy and white matter involvement. An echocardiography at the age of 12 years revealed mild septal hypertrophy. Additionally, hypothyroidism was noted. **Individual 8** is the female cousin of individual 7 and shows an identical course of disease with additional epilepsy. Both individuals never showed neutropenia. The radiological findings of individual 8 are presented in **(Figure 1E-H).**

**3. Severe phenotype (neutropenia, cataracts, infections, total lack of development, three individuals with fetal disease, early death and possible development of leukaemia)**

**Individual 9** was born prematurely at 35 weeks of gestation (wg) and pregnancy was complicated by IUGR. At birth severe generalized hypotonia, bilateral cataracts, a low nasal bridge, hypertelorism and a tented mouth were noted **(Figure 1C).** She suffered severe

drooling and recurrent airway infections as well as otitis media (e.g. pseudomonas aeroguinosa). Chronic severe neutropenia (0.0-0.4 G/L) was noted from the age of three months onwards. Her bone marrow showed maturation arrest at promyelocyte state **(Figure 2).** Continuous treatment with antibiotics, antimycotics and G-CSF as well as gastrostomy and extirpation of saliva glands helped stabilize her clinical condition. She displayed marked developmental delay, never learnt to roll over or to make contact. She had dystonic movements of the hands, feet and perioral and increasing muscle tone of the lower limbs and died at nearly four years of age due to increasing obstructive and central respiratory problems. Her MRI showed cerebellar hypoplasia (the vermis being more affected than the cortical hemispheres) and alterations in globus pallidus and capsula interna as well as white matter alterations in the parieto-occipital region. Evaluation of the oxidative phosphorylation system in fresh muscle and fibroblasts showed no abnormalities.

**Individual 10** was born prematurely (35wg). Since birth he had sucking and swallowing difficulties and recurrent vomiting. At the age of 11 days he was hospitalized with clinical signs of sepsis. Since the second week of life severe neutropenia (<0.5 G/L), monocytosis, and recurrent bacterial infections were noticed. He needed tube feeding due to bulbar paralysis and absent swallowing reflexes. Dysmorphic features were noticed involving high and hairy forehead, hypertelorism, low nasal bridge, retrognathia, dysplastic ears, clinodactyly of the hands and hypospadias, partial T2-3 syndactyly **(Figure 1A).** He had absolute developmental arrest; made no eye or other contact. Brain MRI revealed generalized brain atrophy. At the age of two months hepatosplenomegaly, progressive granulocytopenia and monocytosis were noted, and acute myeloid leukemia (phenotype M5; acute monocytic) was diagnosed. The morphological investigation of bone marrow aspirate showed predominantly dysplastic monocytes and dysplastic granulopoiesis. The karyotype from bone marrow cells was 46,XY(95%)/45,XY,-21/45XY,-7. Chemotherapy was initiated, but after the second course the individual deceased at 3.5 months of age. Upon brain autopsy generalized atrophy and polygyria were noted. His younger sister, **individual 11,** was born normally at term and showed identical dysmorphic features, and an identical course of disease with jaundice and group B streptococcal septicemia at day 3 of life. The same dysmorphic features with her brother were noted **(Figure 1B).** She made no eye contact or showed any development. Brain MRI showed generalized brain atrophy and delayed myelination. She had very weak swallowing and sucking reflexes necessitating tube feeding. Furthermore, she suffered progressive severe neutropenia (<0.5 G/L), monocytosis (33-70%) and hepatomegaly from birth onwards. Bone marrow morphological investigation and immuno-phenotyping was

performed three times. There was a predominance of atypical dysplastic monocytes (33-74%), mature neutrophils were almost absent and 10-15% of blasts cells were present. Myelodysplastic syndrome and pre-leukaemic syndrome were diagnosed with a possibility of myelomonocytaric leukaemia. Following the wish of parents she received only palliative care and died at 3.5 months of age. No autopsy was performed.

P**atient 12** had *in utero* complications including IUGR, decreased placental flow and polyhydramnion and manifested fetal oedema. From the first day of life, significantly increased muscle tension and jaw clenching were noticed ("stiff baby"). Massive limb tremor, generalized seizures resistant to anticonvulsants, and non-epileptic periodical apnea and unconsciousness were observed and persisted through life. Brain ultrasound, ocular fundus examination and neonatal hearing screening were normal. During the neonatal period the girl presented with increasing respiratory failure and feeding problems for which she received parenteral/tube feeding and transiently assisted ventilation. She had severe chronic neutropenia (0.1-0.7 10E9/l) and suffered severe bacterial and fungal infections despite treatment with antibiotics, antimycotics and G-CSF. Bone marrow biopsy showed vacuolar degeneration of the phagocytic mononuclear system (without typical signs of known congenital neutropenia). She showed hardly no development until passing away at five months of age due to an infection with consecutive cardiorespiratory failure. On autopsy microcephaly, marked loss of cellular structures in both hemispheres of the brain and a total depletion of cellular structures of the cerebellum and brainstem were reported.

The pregnancy with **individual 13** was complicated by placental calcifications, polyhydramnion and IUGR and ended at term by Caesarian section due to fetal distress. The newborn period was dominated by signs of respiratory failure, pneumonia and severe leukopenia. The individual presented tetraspasticity and forced flexion of the limbs, furthermore lockjaw (“stiff baby”), nystagmus and trembling of limbs. He died at months of age. The pregnancy of his younger brother, **individual 14,** was complicated by intrauterine jitteriness / seizures. From birth onwards the individual was jittery, unconscious, non reactive, made no contact and showed severe hypertonia (“stiff baby”). Echocardiographic examination revealed mild dilated cardiomyopathy. Head ultrasound showed abnormal brain structures, no details were reported. Additionally, from the 3$^{rd}$ week of life oliguria appeared followed by generalized oedema. Laboratory studies included persistent leukopenia reaching 1.2 G/L with lymphocythosis. Despite intensive medical treatment, the individual passed away at 24 days of age.

**Supplementary material and methods**

*Cell culturing*

Different cell types were cultured under specific conditions for each experiment. Fibroblast cell lines for lipid analysis were cultured in RPMI 1640 medium (Gibco, Breda, The Netherlands) containing 10% (v/v) fetal calf serum (FCS; Sigma, Zwijndrecht, The Netherlands), 1% 10 U/µl Penicillin-10 µg/µl Streptomycin (Gibco, Breda, The Netherlands), and 1% GlutaMAX (Gibco, Breda, The Netherlands). Fibroblasts that were used for assessment of mitophagy and autophagy, were kept in high glucose Dulbecco's Modified Eagle's Medium supplemented with 10% FCS (Lonza, Breda, The Netherlands) and 1% 10 U/µl Penicillin-10 µg/µl Streptomycin (Gibco, Breda, The Netherlands). All fibroblasts were grown at 5% CO2 and a temperature of 37°C.

*First strand synthesis*

RNA was isolated from fibroblast cell lines of affected and control individuals by using the NucleoSpin RNA II kit (Macherey-Nagel, Düren, Germany) according to the manufacturer's protocols. The integrity of the RNA was assessed on 1.2% agarose gel, and the concentration and purity determined by optical densitometry. The $OD_{260}/OD_{230}$ and $OD_{260}/OD_{280}$ ratios were between 1.8 and 2.0. 0.5 µg of total RNA was transcribed into cDNA by using the iScript cDNA synthesis kit (Bio-Rad Laboratories, Hercules, CA, USA) according to the manufacturer's protocol. cDNA was purified by using the NucleoSpin extract II kit (Macherey-Nagel, Düren, Germany) according to the manufacturer's protocol. In case of expression profiling, total RNA from different human adult and fetal tissues was ordered from Stratagene Europe (Amsterdam, The Netherlands). All fetal tissues are from 20 or 21 week-old embryos after gestation, except for cochlear RNA that was isolated from an 8 week-old embryo by using the NucleoSpin RNA II kit (Macherey-Nagel, Düren, Germany) according to the manufacturer's protocols. To remove residual traces of genomic DNA, the cochlear RNA was treated with DNase I (Invitrogen, Leek, The Netherlands) while bound to the RNA binding column. The integrity, concentration, and purity of the RNA were assessed as described above. Of all tissues, 5 µg of total RNA were transcribed into cDNA by using the iScript cDNA synthesis kit (Bio-Rad Laboratories, Hercules, CA, USA) according to the manufacturer's protocol. cDNA was purified by using the NucleoSpin extract II kit (Macherey-Nagel, Düren, Germany) according to the manufacturer's protocol.

*Tissue expression analysis*

q-PCR quantifications were performed in duplicate on the equivalent of 12.5 ng total RNA input. Experimental threshold cycles (Ct) values were within the range of cDNA dilutions used to validate the primers. The melt curves of all PCR products showed a single PCR product. All water controls were negative. *GUSB* and *PPIB* were used as reference genes. Differences in expression of a gene of interest between two samples were calculated as described above.

*Immunofluorescent detection of CLPB*

For immunofluorescent detection of V5 tagged CLPB, U2OS cells were grown on coverslips in six well plates and transiently transfected with a pLenti-CLPB-V5 expression construct using TransIT-LT1 (Mirus, Madison, WI) according the manufacturer's instructions. As a transfection efficiency control we co-transfected with a pTagRFP-H2B (Evrogen). The medium was replaced 4 hrs post-transfection with regular cell culture medium. Cells were fixed using 3.3% paraformaldehyde in cell culture medium for 15 min, washed 3x in PBS and permeabilized for 15 min with 0.5% Triton X100 in PBS/10% fetal calf serum (FCS). Primary V5 monoclonal antibody was diluted 1:100 and incubated in PBS/10%FCS for 1 hr. Secondary goat-anti-mouse IgG AlexaFluor 488 was likewise incubated for 1 hr at a 1:1000 dilution. Slides were mounted using ProLong® Gold antifade with DAPI (Invitrogen). Image acquisition was performed using a Zeiss Observer.Z1with led illumination and appropriate emission filters.

*OXPHOS measurements*

OXPHOS measurements in different tissues were performed as reported earlier. The measurement of the oxygen consumption rate in the presence of pyruvate and malate as mitochondrial respiration substrates was performed as described previously [35].

*Assessment of autophagy and mitophagy*

In all assays, fibroblast passage numbers (<10) were matched. To challenge cellular processes of mitophagy by increasing the amount of dysfunctional mitochondria, fibroblasts were treated with the potassium ionophore valinomycin (1µM for 1h, Sigma-Aldrich, St. Louis, CA, USA). Proteins were extracted using RIPA buffer (50mM Tris-HCl pH7.6, 150mM NaCl, 1% DOC, 1% NP-40) containing 0.1% SDS. Cells were dissolved in the appropriate amount of buffer and incubated on ice for 30 min. Next, lysates were centrifuged at 16,000xg

for 20min at 4oC. The supernatant was transferred into a new tube and used for Western blotting. Western blot analysis was performed as previously published using antibodies raised against β-actin (1:1000000, #A2228, Sigma-Aldrich, St. Louis, CA, USA), GRP75 (1:1000000, #ab2799, Abcam, Cambridge, UK), LC3 (1:1000, #4108, Cell Signaling Technology, Boston, MA, USA)[36].

*Lipid analysis*

Fibroblast cell lines were harvested by centrifugation at 200xg for 5 min at room temperature, washed once with PBS, pelleted by centrifugation at 200xg for 5 min at room temperature, and snap frozen in liquid nitrogen. Levels of the following phospholipids were analyzed: phosphatidylglycerols (PG), bis(monoacylglycerol)phosphate (BMP), phosphatidic acids (PA), phosphatidylcholines (PC), phosphatidylethanolamines (PE), phosphatidylserines (PS) phosphatidylinositols (PI), cardiolipins (CL), sphingomyelines (SM) and their lyso-analogue species. The relative abundances of the species in the sample-extracts were determined by HPLC-MS/MS using a Surveyor HPLC system hyphenated to a TSQ Quantum AM tandem mass spectrometer (Thermo Finnigan Corporation, San Jose, CA, USA). The MS was operated alternating in the negative- and positive ion electrospray ionization (ESI) mode in consecutive runs as described in detail previously [37]. Acyl-chain compositions were determined by the product-ion scans of the respective *quasi* molecular ions.

*Analysis of CLPB and HAX1 protein interactions*

Data on proteins that physically interact with CLPB (**Table S4**) were retrieved from public databases (BioGRID, Biological General Repository for Interaction Datasets; HPRD, Human Protein Reference Database; MINT, Molecular Interactions Database; STRING, Search Tool for the Retrieval of Interacting Genes/Proteins). Database information on physical protein interactions for HAX1 was obtained from the most recent release from the BioGRID database (www.thebiogrid.org/download.php; compiled on October 25$^{th}$ 2014).

In addition, a live cell protein interaction screen of CLPB against a library of $n$ = 100 proteins was performed using bioluminescence resonance energy transfer (BRET), as described before[38; 39]. Briefly, we generated a protein library enriched for gene ontology (GO) tags linked to functions and processes that are associated with 3-MGA-uria[3; 4]. Proteins were selected from a library of n > 500 proteins based on the number of associations with GO biological_process (phospholipid biosynthetic process, cholesterol homeostasis, lipid metabolic process, response to calcium ion, calcium ion binding, membrane organization) and

GO cellular_component (endoplasmic reticulum, mitochondrion, peroxisome, Golgi apparatus, integral to membrane).

BRET protein-protein interaction assays were performed in transfected COS-7 cells as described before[38; 39]. Full-length open reading frames of genes encoding CLPB (BC 006404.2) and genes encoding proteins of the $n = 100$ library were introduced into plasmid vectors for the expression of amino- and carboxy-terminal fusions with Rluc or YFP. All eight possible combinations of Rluc (donor) or YFP (acceptor) fusions tagged at the amino or carboxyl terminus were tested in duplicates for each putative interaction pair at an acceptor/donor ratio of 3:1. BRET ratios were calculated by the equation $R = (I_A / I_D) - cf$, where $R$ is the BRET ratio, $I_A$ is the BRET signal, $I_D$ is the Rluc signal and $cf$ is a correction factor ($(I_A / I_D)_{control}$), with co-transfection of the donor fusion protein with YFP in the absence of the second protein of interest used as the control. Protein interactions were assumed to be true positive, if the BRET ratio of at least one combination of acceptor and donor tagged interaction pairs exceeded a method-specific threshold of 0.0263. The threshold for classification of positive protein interactions was generated by measurement of two libraries of $n = 60$ proteins with known positive protein interactions (positive reference set, PRS) and putatively negative protein interactions (random reference set, RRS), as described previously [40].

**Supplementary tables and figures**

Table S1. Primer sequences for Sanger Sequencing of *CLPB* (NM_030813.4)

| Exon | Forward primer (5'→3') | Reverse primer (5'→3') |
|---|---|---|
| 1 | caggaaacagctatgaccGGCAGCCATGTTGGACGTGG | tgtaaaacgacggccagtAGTTAGGACAATCTTCCCGCC |
| 2 | caggaaacagctatgaccGTACTGCCACTGTCTTAGTGG | tgtaaaacgacggccagtTCCAAAGCAAAGTCATCACACG |
| 3 | caggaaacagctatgaccCACACCAGGTGGGAGAGTGC | tgtaaaacgacggccagtCAGATGTCAAGCCATACACTG |
| 4 | caggaaacagctatgaccTCCGGATCTGGGTCTGTACC | tgtaaaacgacggccagtACAGAGGTAAAGAACATGCAGG |
| 5 | caggaaacagctatgaccTCTGGGGGTAGAGGGCTTGG | tgtaaaacgacggccagtAAAGAGATAGTCAGATGAGACC |
| 6 | caggaaacagctatgaccGGAGGATAACAGGGCTCTGG | tgtaaaacgacggccagtTGCCTCTTCTTACCCAGCAC |
| 7 | caggaaacagctatgaccGAAATCAGAGCCTTAAGCCACC | tgtaaaacgacggccagtAGTGAAGGATTAAATGATGCATGG |
| 8 | caggaaacagctatgaccCTATGAAGCAGGACCCCTGG | tgtaaaacgacggccagtATCCAGTTTGGTGACGACAGG |
| 9 | caggaaacagctatgaccATACTTAGTGATAATTATCCTGCC | tgtaaaacgacggccagtGGAGGCCGTTGCTTTTAGAGC |
| 10 | caggaaacagctatgaccTGCGCCTCAACATTCTCATCC | tgtaaaacgacggccagtTTCAGAGGGTCAGATTTTTTGGG |
| 11 | caggaaacagctatgaccGGGATAGTTGAGGTGCTCTCC | tgtaaaacgacggccagtTGAGGCCCAAATGACAAGACC |
| 12 | caggaaacagctatgaccTCTCTGTTGAGAGAGGCAACC | tgtaaaacgacggccagtGAATGACCAGCTAGCCTCTGG |
| 13 | caggaaacagctatgaccGGAGGTGAGAACTGAGAGTGC | tgtaaaacgacggccagtAGCTAGGGACAGAGCTGCCC |
| 14 | caggaaacagctatgaccTTTCCATGGGCAGGCCAAGG | tgtaaaacgacggccagtGGCTTCCAGATCTTTAGGATGG |
| 15-16 | caggaaacagctatgaccTGGTAATTTCCCTAACCCGC | tgtaaaacgacggccagtCAAGCTATAGGGAGGCAGGC |
| 17 | caggaaacagctatgaccGGTCTCTGAGTTGCCCTAGC | tgtaaaacgacggccagtAGGCCTGAGACTGGGTAGAG |

Overview of the PCR primers used to amplify the exons of the *CLPB* gene (NM_030813.4). All primers contained a M13 sequence at the 5'end that allowed for sequencing of the PCR products using universal M13 primers.

Table S2. Primer sequences of primers used for QPCR analysis of *CLPB* (NM_030813.4)

| | Forward primer (5'→3') | Reverse primer (5'→3') |
|---|---|---|
| *GUSB* (NM_000181.1) | agagtggtgctgaggattgg | ccctcatgctctagcgtgtc |
| *PPIB* (NM_000942.4) | cggaaagactgttccaaaaac | gattacacgatggaatttgctg |
| *CLPB* (NM_030813.4) | tgaataaagaaatgtaaagg | ttaataaattaaaattatag |

Table S3

| | parameter | Individual 6 | Individual 9 | reference value | unit |
|---|---|---|---|---|---|
| muscle | ATP + CrP production rate | 28,8 | ND | 15.4 - 30.2 | nmol ATP.$h^{-1}$.(mU CS)$^{-1}$ |
| | pyruvate oxidation rate | 3,01 | 1,96 | 1.74 - 3.11 | nmol $CO_2$.$h^{-1}$.(mU CS)$^{-1}$ |
| | complex I | 69 | 102 | 47 - 154 | mU.(mU CS)-1 |
| | complex II | 247 | 230 | 134 - 354 | mU.(mU CS)-1 |
| | complex III | 954 | 969 | 696 - 1756 | mU.(mU CS)-1 |
| | complex IV | 1381 | 1189 | 470 - 1842 | mU.(mU CS)-1 |
| | complex V | 358 | 349 | 161 - 711 | mU.(mU COX)-1 |
| | complex II+III | 347 | 308 | 176 - 492 | mU.(mU CS)-1 |
| | citrate synthase | 238 | 187 | 84 - 365 | mU.(mg protein)-1 |
| fibroblasts | complex I | 342 | 318 | 163 - 599 | mU.(mU CS)-1 |
| | complex II | 465 | 435 | 335 - 888 | mU.(mU CS)-1 |
| | complex III | 850 | 694 | 570 - 1383 | mU.(mU CS)-1 |
| | complex IV | 604 | 537 | 288 - 954 | mU.(mU CS)-1 |
| | complex V | 711 | 635 | 193 - 819 | mU.(mU CS)-1 |
| | complex II+III | 267 | 263 | 128 - 534 | mU.(mU CS)-1 |
| | citrate synthase | 302 | 370 | 151 - 449 | mU.(mg protein)-1 |

ND = not determined, P = individual.

Evaluation of the oxidative phosphorylation in fresh muscle and cultured fibroblasts

Table S4

| | Database | Method | Reference |
|---|---|---|---|
| COPS6 | STRING | Affinity Capture-MS | [41] |
| COPS6 | BioGRID | | |
| CUL3 | BioGRID | Affinity Capture-MS | [42] |
| ERCC6L | BioGRID | Affinity Capture-MS | Huttlin EL (2014/pre-pub) |
| HDAC11 | BioGRID | Affinity Capture-MS | [43] |
| IRS4 | BioGRID | Affinity Capture-Luminescence | [44] |
| IRS4 | BioGRID | Affinity Capture-MS | [44] |
| MDFI | IntAct | Two-hybrid | [45] |
| MDFI | BioGRID | | |
| MGEA5 | BioGRID | Affinity Capture-MS | * |
| OSBPL10 | STRING | Affinity Capture-MS | [41] |
| SMAD9 | HPRD | Two-hybrid | [46] |
| SMAD9 | IntAct | | |
| SMAD9 | MINT | | |
| TERF2 | BioGRID | Affinity Capture-MS | [47] |
| TSEN2 | BioGRID | Affinity Capture-MS | * |
| TTF2 | HPRD | Affinity Capture-MS | * |
| TTF2 | STRING | Two-hybrid | [48] |
| UBC | BioGRID | Affinity Capture-MS | [49] |
| UCHL3 | STRING | Affinity Capture-MS | [41] |
| UCHL3 | BioGRID | Affinity Capture-MS | * |
| USP30 | STRING | Affinity Capture-MS | Sowa ME (2009) |
| USP30 | BioGRID | | |
| RG9MTD1 | STRING | CoIP | [50] |
| STIP1 | STRING | CoIP | [51] |

Direct interaction partners of CLPB as identified by database searches.

* http://thebiogrid.org/166968/publication/high-throughput-proteomic-mapping-of-human-interaction-networks-via-affinity-purification-mass-spectrometry.html (Huttlin EL et al. High Throughput proteomic mapping og human interaction networks via affinity-purification mass spectrometry (pre-publication).

Table S5

| # | Interaction partner | BRET pair | | BRET Ratio | |
|---|---|---|---|---|---|
| | *Name* | *Protein_1* | *Protein_2* | *1st experiment* | *2nd experiment* |
| 1 | ABCD4 | CLBP-C-Venus | ABCD4-C-hRluc | 0,019 | 0.035 * |
| 2 | AGXT | CLBP-C-Venus | AGXT-C-hRluc | 0.028 * | 0.037 * |
| 3 | ATP2A2 | CLBP-N-Venus | ATP2A2-N-hRluc | 0.028 * | 0,000 |
| 4 | CARD8 | CLBP-N-Venus | CARD8-N-hRluc | 0.051 * | 0.059 * |
| 5 | CYB5 | CLBP-N-hRluc | CYB5-C-Venus | 0,020 | 0.027 * |
| 6 | FAR1 | CLBP-N-hRluc | FAR1-C-Venus | 0,013 | 0.027 * |
| 7 | FASN | CLBP-N-hRluc | FASN-N-Venus | 0,013 | 0.027 * |
| 8 | FIS1 | CLBP-N-hRluc | FIS1-C-Venus | 0.055 * | 0.033 * |
| 9 | HMGCL | CLBP-C-Venus | HMGCL-C-hRluc | 0,000 | 0.029 * |
| 10 | IL1B | CLBP-N-hRluc | IL1B-N-Venus | 0.027 * | 0,026 |
| 11 | MIF | CLBP-N-hRluc | MIF-C-Venus | 0.051 * | 0,025 |
| 12 | MPV17L2 | CLBP-N-hRluc | PEX19-N-Venus | 0.050 * | 0.062 * |
| 13 | NLRP2 | CLBP-N-hRluc | PEX5isob-N-Venus | 0.056 * | 0.054 * |
| 14 | PEX19 | CLBP-N-hRluc | PYCARD-C-Venus | 0.062 * | 0.057 * |
| 15 | PEX5isob | CLBP-N-hRluc | RIPK2-N-Venus | 0.030 * | 0,025 |
| 16 | PYCARD | CLBP-N-Venus | SSR1-C-hRluc | 0,000 | 0.037 * |
| 17 | RIPK2 | CLBP-N-Venus | MPV17L2-N-hRluc | 0.037 * | 0,000 |
| 18 | SSR1 | CLBP-N-hRluc | NLRP2-N-Venus | 0.030 * | 0,002 |
| 19 | SERAC1 | SERAC1-N-Venus | CLBP-N-hRluc | 0.028 * | 0.027 * |

Proteins interacting with CLPB as determined by BRET. A live-cell screen of CLPB against a library of 100 proteins by means of bioluminescence resonance energy transfer (BRET) identified 19 positive interactions. The library of 100 proteins was derived from a random library by enrichment for proteins associated with the Gene Ontology (GO) annotations biological_processes phospholipid biosynthetic process, cholesterol homeostasis, lipid metabolic process, response to calcium ion, calcium ion binding, membrane organization, and GO cellular_components endoplasmic reticulum, mitochondrion, peroxisome, Golgi apparatus, integral to membrane. The protein interaction pairs are given and the orientation (C, C-terminus; N, N-terminus) of BRET tags (Venus, variant of yellow fluorescent protein; Rluc, Renilla luciferase) is indicated. Protein interactions were assumed as true positive, if the BRET ratio of at least one experiment exceeded a method specific threshold of 0.0263 (indicated by *).

Figure S1

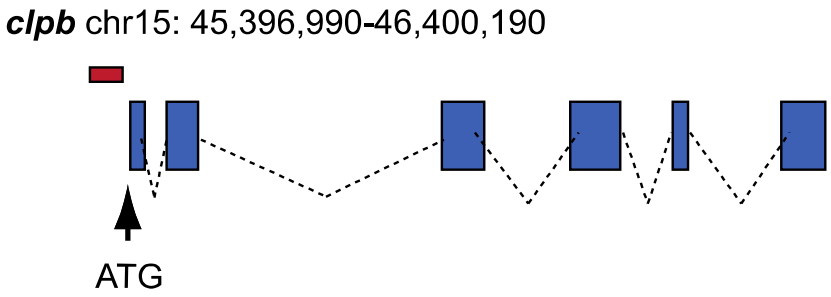


Schematic representation of the *D. rerio clpb* locus. Blue, exons; dashed lines, introns; white, untranslated regions; red box, MO; ATG indicates the translation initiation site.

Figure S2

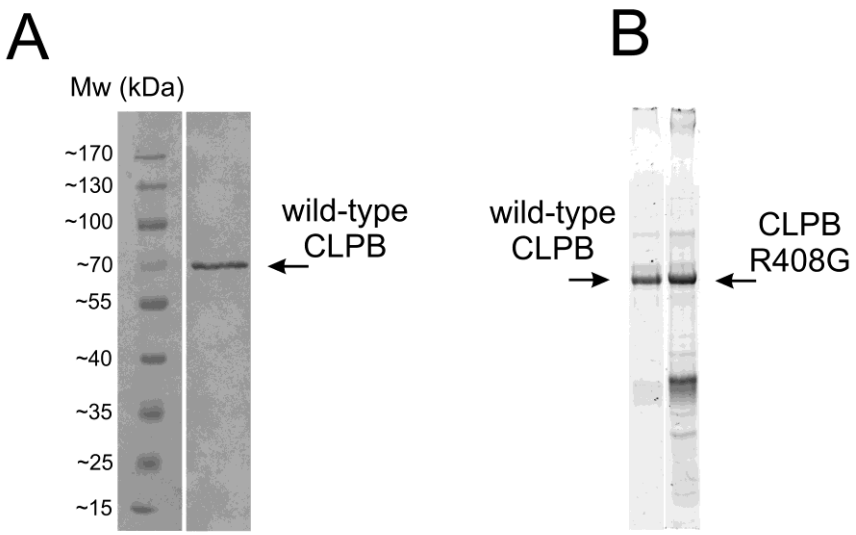


Preparations of CLPB protein and its p.Arg408Gly (R408G) variant. (A) Western blot of purified wild type CLPB protein with an anti-CLPB antibody (Abcam ab87253). B) SDS-PAGE of purified wild type and p.Arg408Gly CLPB sample (Biorad 12% TGX StainFree FastCast gel, visualised with Biorad ChemiDoc MP).

.

Figure S3

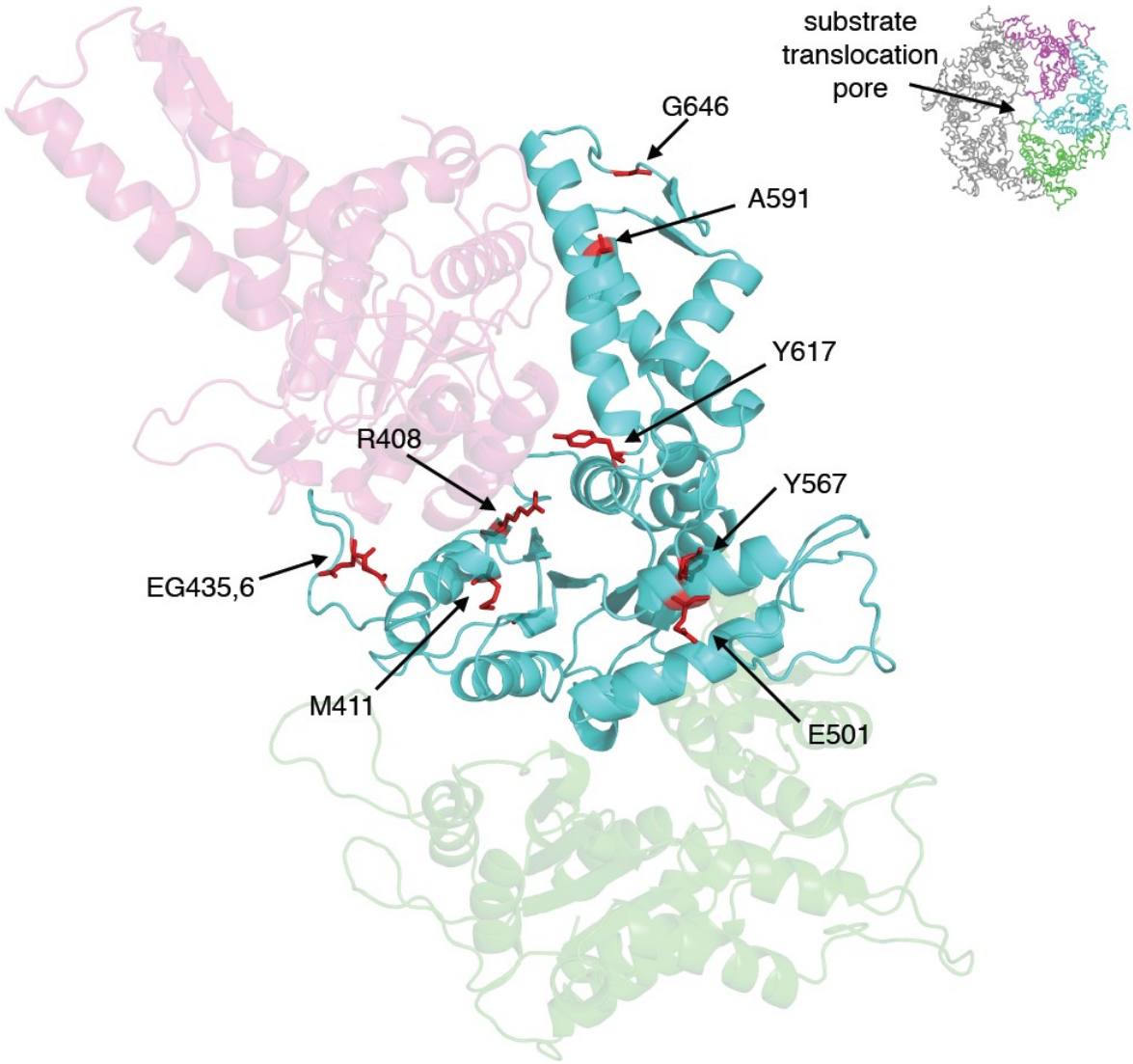


Residues affected by missense mutations in the predicted CLPB protein structure (cyan). Two neighboring subunits (magenta and green) are shown, together with the position of the three subunits in the CLPB hexamer (insert). The structural model shown is based on *T. thermophilus* ClpB (pdb:1qvr) and prepared using and PyMOL (www.pymol.org) [52].

Figure S4

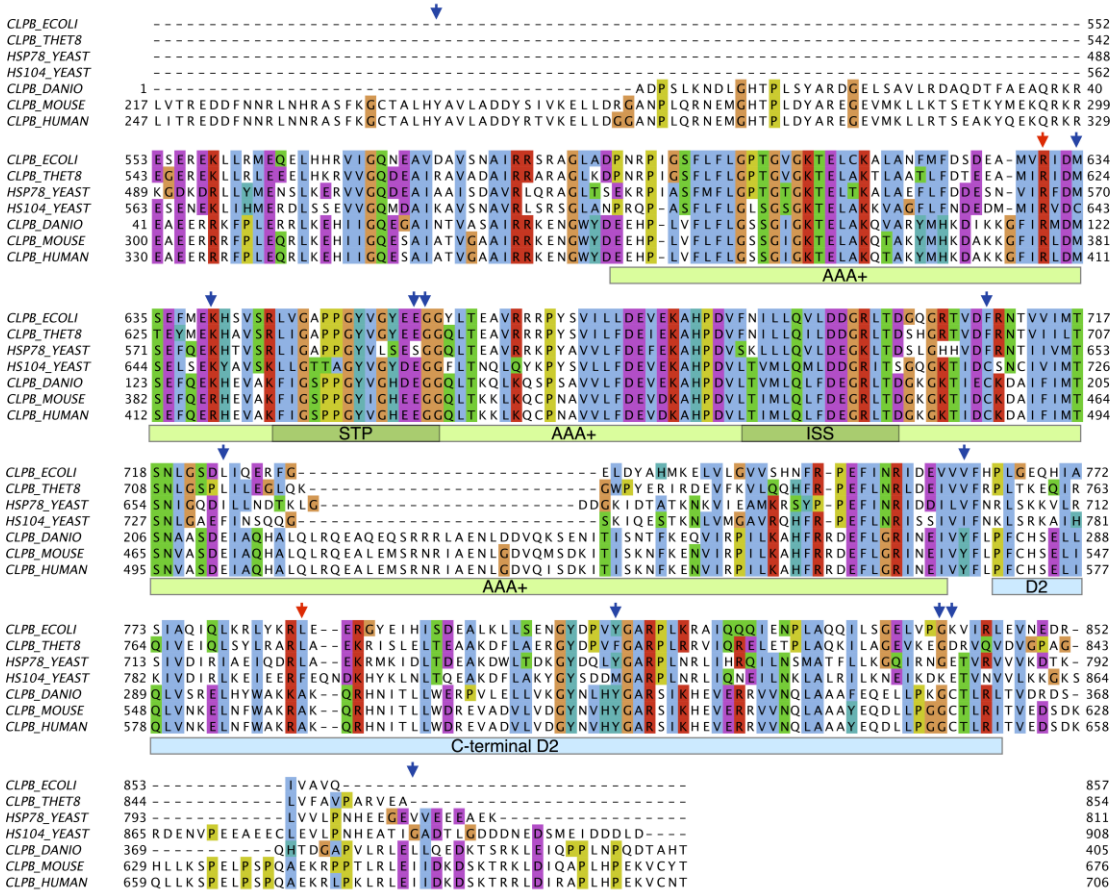


Alignment of the conserved region of human CLPB protein with its bacterial (*E. coli* and *T. thermophilus*), fungal (mitochondrial HSP78 and cytosolic HSP104) as well as vertebrate orthologs [zebrafish (*Danio rerio*) and mouse (*Mus musculus*)]. Arrows denote missense mutations in our cohort of individuals (blue: heterozygous, red: homozgous). Protein domains in the human sequence are marked under the alignment. AAA+ - ATPase domain, C-terminal D2 - CLPB-specific domain not present in other proteins from CLPA/C/X families. The C-terminal domain is essential for oligomerization, stabilizing the functional assembly [53; 54]. Structural motifs are highlighted in the alignment: STP - Substrate Translocation Pore (ISS - Inter-Subunit Signaling) motifs regulating ATP power-stroke for substrate translocation [32; 55]. In parenthesis the total length of the sequences is given.

Figure S5

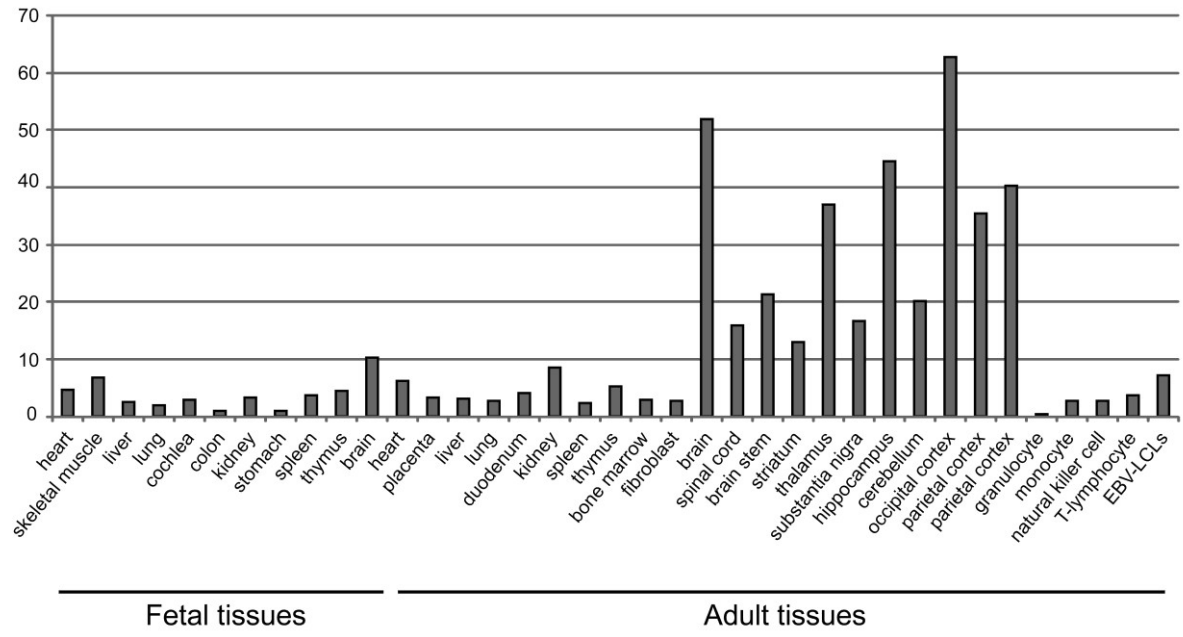


Expression of *CLPB* by mRNA expression analysis in human fetal and adult tissues. Relative expression levels are given as the fold change in comparison to the tissue with the lowest expression level. Quantifications were performed in duplicate and normalized against GUSB. Differences in expression between tissues were calculated by the comparative Ct or $2^{\Delta\Delta Ct}$ method [56; 57].

Figure S6

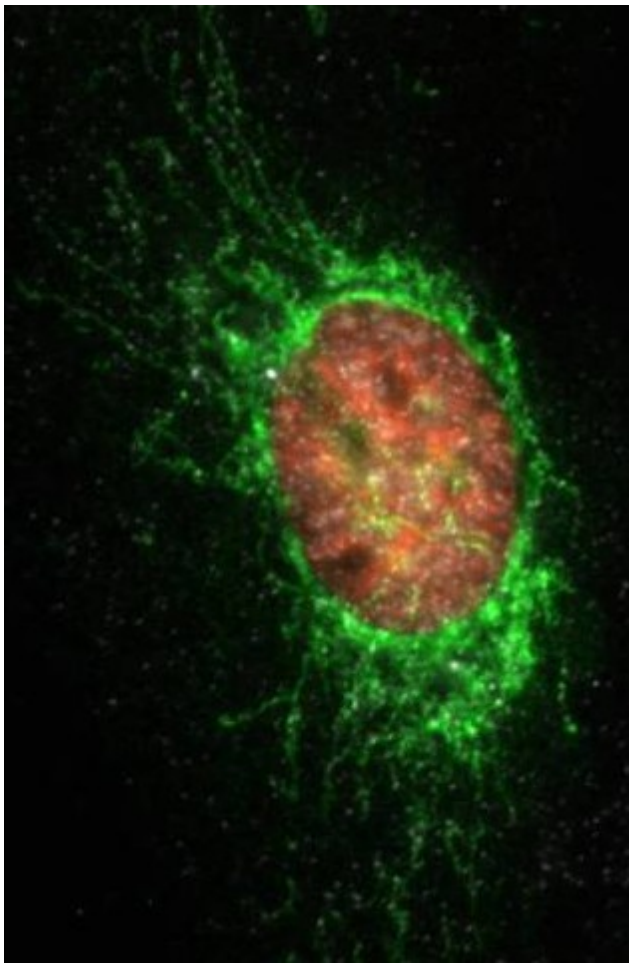

Subcellular localization of CLPB. U2OS cells were transiently transfected with CLPB-V5 and pTagRFP-histone H2B expression constructs. CLPB-V5 (green) as well as HSP60 (white) were detected by immunofluorescence and showed mitochondrial co-localization distinct from the nuclear H2B fluorescence (red).

Figure S7

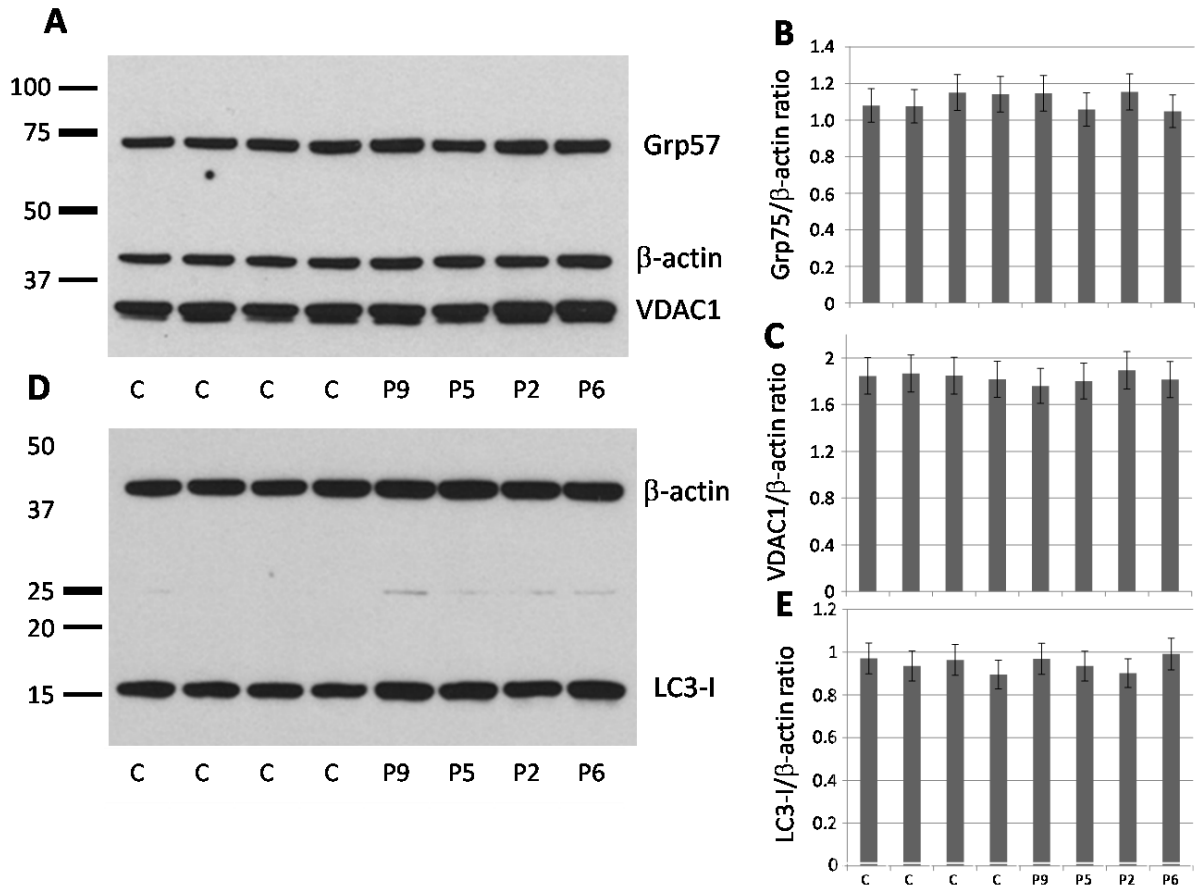


Autophagy flux and mitochondrial clearance. (A,B,C) Mitochondrial clearance or mitophagy in fibroblasts under basal conditions was evaluated by measuring the mitochondrial proteins Grp75 and VDAC1 after immuno-blotting on SDS gels. β-Actin served as a loading control. Evidence for the presence or absence of mitophagy was based on the ratio of the two mitochondrial markers over β-actin in four individual cell lines (#9, 5, 2, 6) and four controls. No significant differences were observed. (D,E) Autophagy in fibroblasts was measured under basal conditions. We used the conversion of LC3 from its cytosolic form LC3-I (~17kDa) to the autophagy-relevant form LC3-II (~15kDa), a commonly used indicator of autophagy. The LC3 forms were separated on SDS gels and after immunoblotting expressed as ratio over β-actin using densitometry. No significant differences were found using four affected individual cell lines (#9,5,2 and 6) and 4 controls.

Figure S8

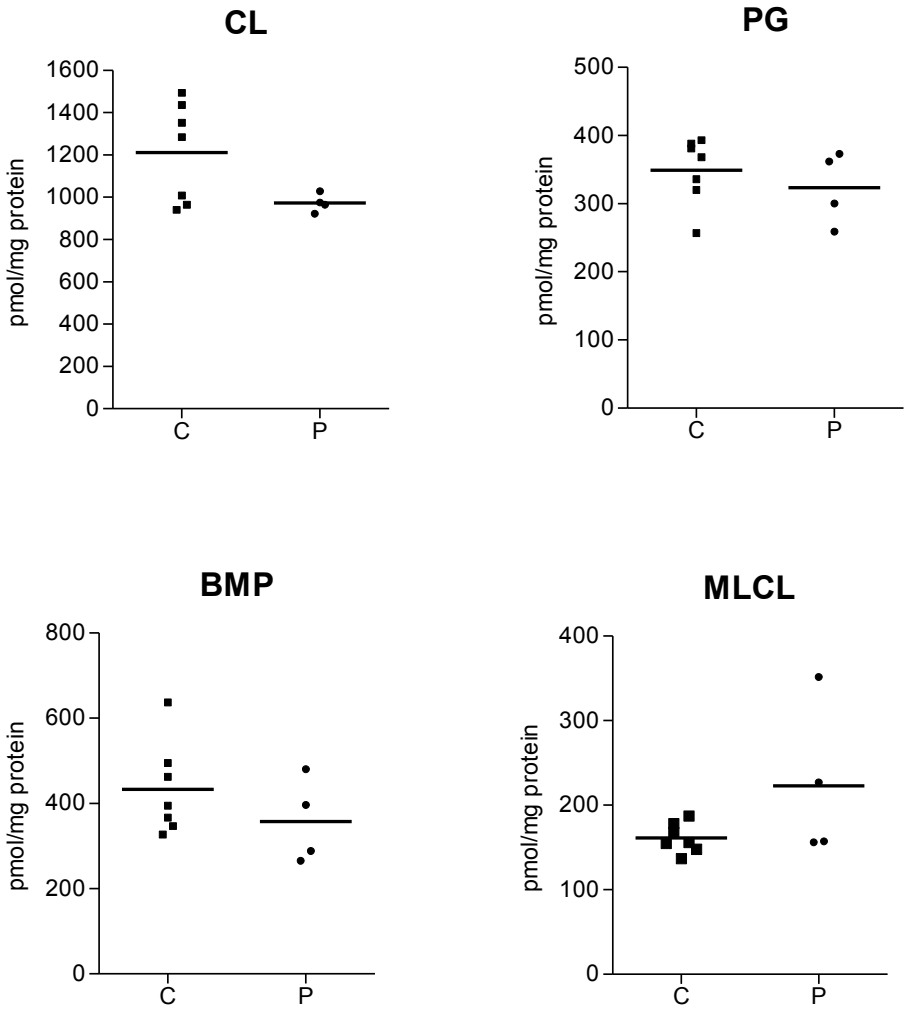


Scatter plots of the total levels of cardiolipin (CL), phophatidylglycerol (PG), bis(monoacylglycerol)phosphate (BMP) and monolyso-cardiolipin (MLCL) in controls (n=7) and affected individuals (n=4). Statistical significance was assessed using a two-tailed student's t-test (CL (p=0.037), MLCL (p=0.273), PG (p=0.467) and BMP (p=0.283).

Figure S9

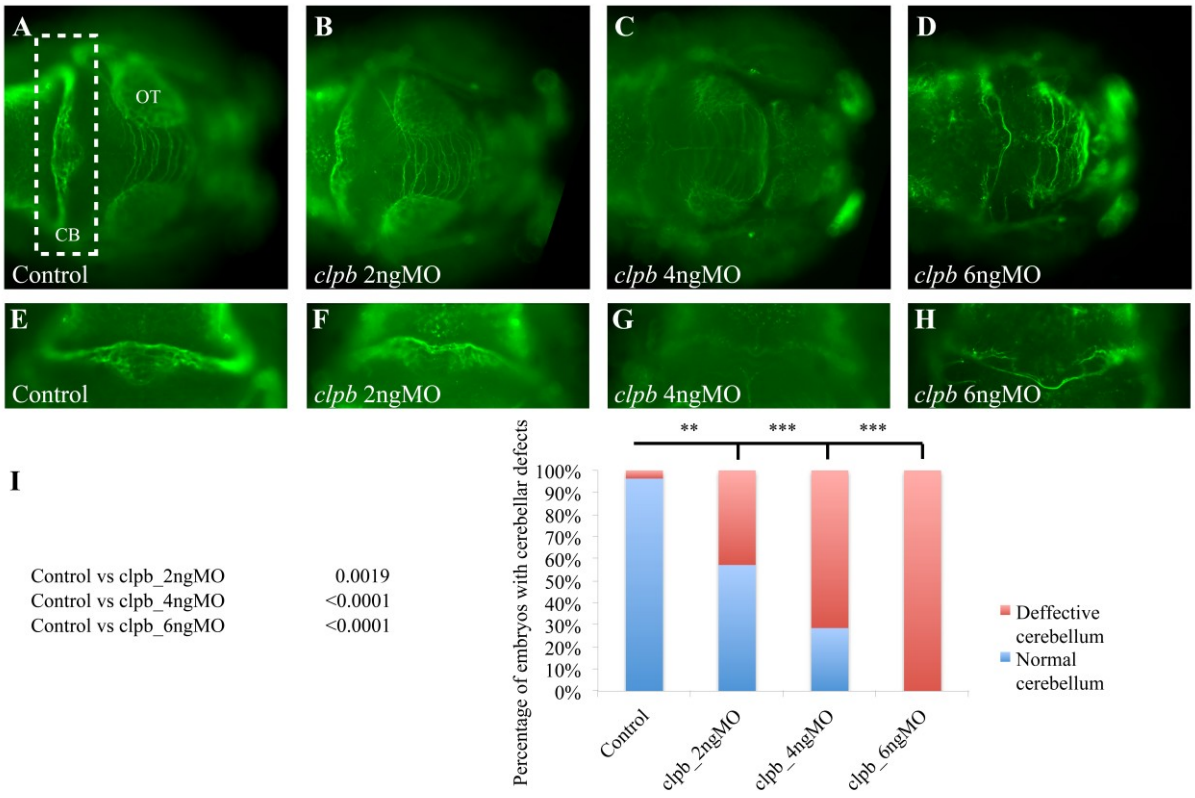


(A-D) Dorsal view of the brain stained with acetylated tubulin in 3 days post fertilization (dpf) in developing zebrafish embryos. A progressive disorganization of the CNS is observed with increasing doses of a translation-blocking morpholino (MO) against *clpb* (TB-*clpb*). More specifically, embryos injected with higher doses of MO show microcephaly, reduction of the size of the optic tectum (OT; a structure equivalent to the superior culliculus in humans), and degeneration of the axons forming the cerebellum (CB). (E-H). Magnifications of the cerebellum, highlighted with the white dashed line in panel A. (I) p-values and quantification of the embryos showing defects in the cerebellum across progressively increasing doses of MO.

Figure S10

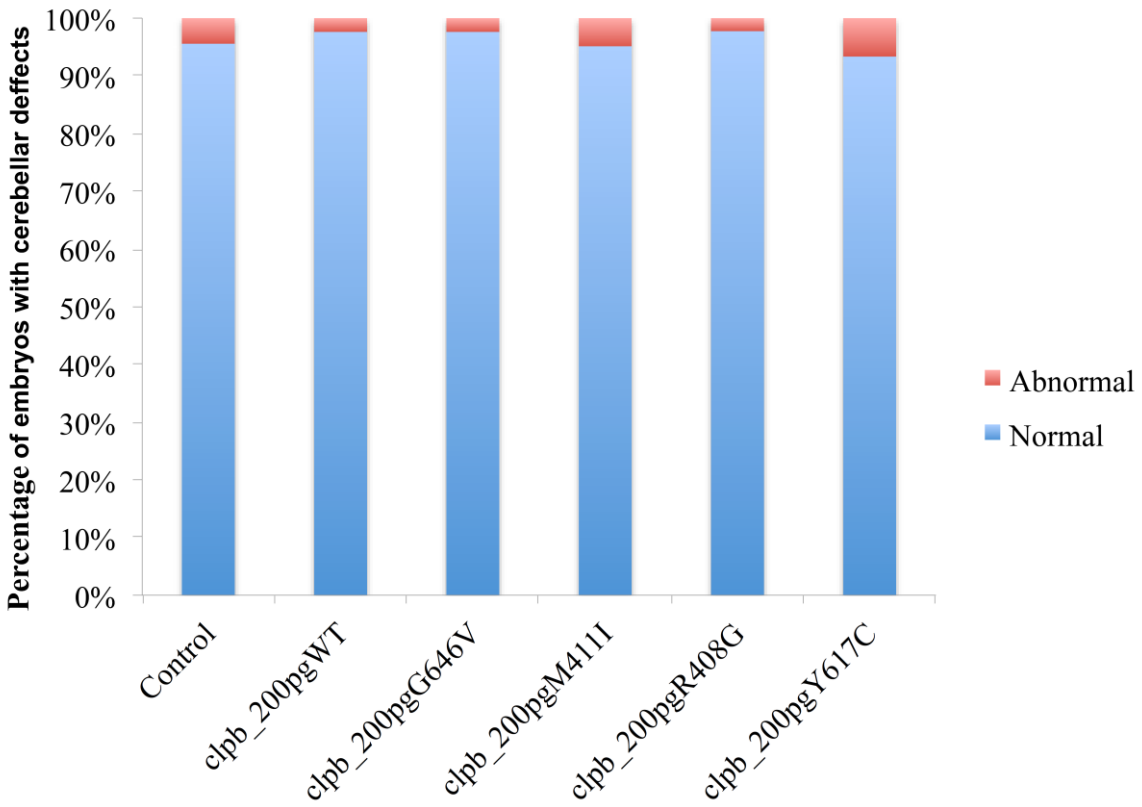


Overexpression of the non-synonymous *CLPB* alleles tested with the *in vivo* functional model. Overexpression of wt *CLPB* mRNA or *CLPB* mRNA harboring any of the variants identified in the study cohort does not lead to changes in the integrity of the cerebellum in zebrafish embryos at 72 hpf, suggesting that injection of each of the mutant constructs alone does not lead to toxicicity and induction of a phenotype similar to the morpholino.

Figure S11

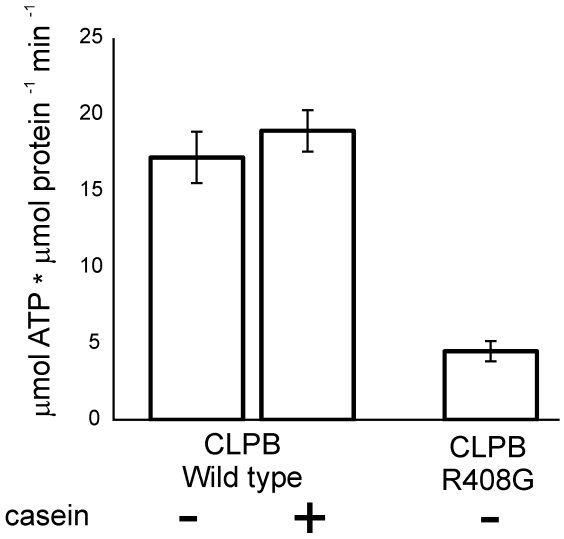


ATPase activity of purified wildtype and p.Arg408Gly (R408G) ClpB. All measurements were run in triplo. Mutant ClpB had 26% ATPase activity compared to wild type human ClpB.